

https://dspace.org/

Development of Energy Management Strategies for Port Cranes

Takalani, Rofhiwa Lutendo Edward

2025
University of the Witwatersrand, Johannesburg
https://hdl.handle.net/10539/50095
Takalani, Rofhiwa Lutendo Edward. (2025). Development of Energy Management Strategies for Port Cranes. [PhD thesis, University of the Witwatersrand, Johannesburg]. WIReDSpace. https://hdl.handle.net/10539/50095

Downloaded from a DSpace repository. https://dspace.org/



Development of Energy Management Strategies for Port Cranes

Rofhiwa Lutendo Edward Takalani

A thesis submitted to the Faculty of Engineering and the Built Environment, University of the Witwatersrand, Johannesburg, in fulfilment of the requirements for the degree of

Doctor of Philosophy

2025

Declaration

I declare that this thesis report is my own original work, submitted to the University of the Witwatersrand for the degree of Doctor of Philosophy. This work has not been submitted to any institute of learning for a degree.



_____

Rofhiwa Lutendo Edward Takalani

Student Number: 578584

Braamfontein, Johannesburg

June, 2025

Dedication

To my parents:

Thabelo Joel Takalani

And

Nkhangweleni Ethel Sivhidi

Acknowledgements

I would like to express my deepest gratitude to my supervisor Dr. Lesedi Masisi, for his invaluable guidance, patience, and encouragement throughout this journey. Dr. Masisi's insightful feedback and unwavering support has been instrumental in shaping this research.

To my wife, Takadzani Takalani, thank you for your love, unwavering support, patience, and understanding during both the enjoyable and challenging moments of this journey. I am also very grateful to my children, Michael and Abigail, for showing interest in my PhD, as well as their support and encouragement.

I dedicate this work to my parents who, through poverty and great difficulty, worked extremely hard and sacrificed everything to give me an education and a better life; I am eternally grateful.

Finally, I give thanks and praise to Jesus Christ, my Lord, God, and Savior.

Abstract

This study focuses on developing an energy management strategy and an optimal load-handling trajectory for port cranes, specifically Ship-to-Shore (STS) cranes. The objective is to minimise load cycle time, optimise the crane's energy consumption, and reduce its reliance on the grid. This is achieved by applying a battery-supercapacitor hybrid energy storage system (H-ESS), and a combination of filtering and Pontryagin's Minimum Principle (PMP) energy management strategies (EMSs). The port crane system model is developed using the graphical energetic macroscopic formalism (EMR). The filtering-based EMS manages the power split between the grid and the H-ESS, while the PMP-based EMS manages the power split between the battery and supercapacitor within the H-ESS. Overall, the proposed EMS for this study has a simple analytical cost function, is computationally fast, and is easy to implement while producing optimal and effective results. The EMR-based port crane model is comprised of mathematical equations describing the crane systems, the cranes' local control system, and a MATLAB Simulink simulation model.

The experimental validation of the EMR-based port crane model is conducted by comparing the MATLAB Simulink simulations with real-world crane data. The results show that implementing the EMS reduces the port crane energy consumption from the utility grid by 29% and decreases peak power consumption by 29.6%. During the crane load handling cycle, the supercapacitor and the battery discharge and recharge by 26% and 8%, respectively. Simulations also show that the developed optimal crane load trajectory is 38% faster and more productive than the non-optimal crane load trajectory. Additionally, the results show that the optimal trajectory reduces the cranes' peak power and energy consumption by 36% compared to the non-optimal trajectory. Furthermore, the EMS enhances the performance of the H-ESS by boosting efficiency, improving reliability, and extending its lifespan, making H-ESS more dependable and cost-efficient. Given that STS cranes are the largest port cranes, with power demands of about 2 MW, and share a common drivetrain with many types of port and industry cranes, the EMS developed in this study can be applied to other types of cranes. Lastly, the study presents a generalised port crane H-ESS sizing framework that uses the optimal EMS and particle swarm optimisation (PSO) algorithm to determine the optimal sizes for the battery and supercapacitor packs in the H-ESS.

Academic Papers

Journals

1. Takalani, R.L.E.; Masisi, L. Development of an Optimal Port Crane Trajectory for Reduced Energy Consumption. *Energies* **2023**, *16*, 7172. https://doi.org/10.3390/en16207172

2. Takalani, Rofhiwa, and Lesedi Masisi. "Energy Consumption Optimization Strategy for Port Cranes Based on Pontryagin's Minimum Principle and Filtering Strategies." IEEE Access (2025).

Conferences

1. Takalani, R., & Masisi, L. (2021, October). Development of An Energy Management Strategy for Port Cranes. In *IECON 2021–47th Annual Conference of the IEEE Industrial Electronics Society* (pp. 1-6). IEEE.

2. Takalani, R., & Masisi, L. (2022, June). Energetic macroscopic representation based electric bus modelling and energy management strategy. In *2022 IEEE 31st International Symposium on Industrial Electronics (ISIE)* (pp. 955-958). IEEE.

Table of Contents

LIST OF FIGURES ..... **IX**

LIST OF TABLES ..... **XI**

NOMENCLATURE ..... **XII**

1. INTRODUCTION **1**

2. BACKGROUND **3**

2.1 Scientific Context of This Study 3

2.2 Thesis Objective and Approach 4

2.2.1 Research Objectives *4*

2.2.2 Research Questions *4*

2.2.3 Methodology *4*

2.3 Chapter Summary 6

3. LITERATURE REVIEW **7**

3.1 Literature Review 7

3.1.1 Studied Port Crane System *7*

3.1.2 Gaps in Literature *8*

3.2 Review of Energy Management Strategies 10

3.3 Chapter Summary 14

4. PORT CRANE SYSTEM MODELLING **16**

4.1 Port Crane Electromechanical System Description 16

4.2 Port Crane Energetic Macroscopic Representation 18

4.3 Port Crane Mathematical Modelling 19

4.4 System Disturbances 19

4.5 Port Crane Local Control System 21

4.6 Port Crane System Model Experimental Validation 22

4.6.1 Experimental Setup *22*

4.6.2 Experimental Results *24*

4.7 Chapter Summary 25

5. DEVELOPMENT OF THE OPTIMAL PORT CRANE TRAJECTORY **26**

5.1 Description of The Port Crane Load Handling Mechanism 26

5.2 Optimal Port Crane Trajectory 27

5.3 Port Crane Optimal Power Consumption 33

5.4 Optimal vs. Non-Optimal Trajectory 36

5.5 Simulation Results 38
5.6 Chapter Summary 40

6. ENERGY CONSUMPTION OPTIMIZATION STRATEGY FOR PORT CRANES BASED ON PONTRYAGIN'S MINIMUM PRINCIPLE AND FILTERING STRATEGIES 41

6.1 Port Crane System EMR-based Model 41
6.2 H-ESS Mathematical Modelling 42
6.3 Proposed PMP-based Energy Management Strategy 43
6.3.1 Problem Formulation 45
6.3.2 EMS Development Using PMP 47
6.3.3 PMP EMS Implementation 50
6.4 Proposed Filtering-based Grid/H-ESS Energy Management Strategy 51
6.4.1 H-ESS Model Reduction 51
6.4.2 Filtering EMS development 52
6.4.3 Braking Strategy 53
6.4.4 Filtering And Braking Strategies Implementation 54
6.5 EMS Strategy Implementation 56
6.6 Chapter Summary 57

7. OPTIMAL SIZING OF THE PORT CRANE'S BATTERY/SUPERCAPACITOR H-ESS 59

7.1 Battery and Supercapacitor Models 59
7.2 Generalised Port Crane H-ESS Sizing Framework 61
7.3 Generalised H-ESS Sizing Problem Formulation 62
7.4 Constraints 63
7.5 PSO H-ESS Sizing Algorithm 64
7.6 Simulation Results 65
7.7 Chapter Summary 69

8. CONCLUSIONS AND FUTURE WORKS 70

8.1 Conclusions 70
8.2 Recommendations for Future Works 71

BIBLIOGRAPHY 72

List of Figures

Figure 1.1: Port terminal overview 1

Figure 2.1: Scientific context of this study 3

Figure 2.2: Thesis methodology 5

Figure 3.1: Port crane motions (a), port crane drivetrain (b) 7

Figure 3.2: Port crane powertrain 8

Figure 3.3: Classification of energy management methods [21] 11

Figure 4.1: Studied port crane system 16

Figure 4.2: Port crane EMR and inversion-based local control 18

Figure 4.3: Port crane local control system 21

Figure 4.4: Experimental setup (a) and (b): (1) Hoist motor (2) Fluke 1736 power logger (3) Cable drum (4) Gearbox (5) Mechanical brakes (6) PC, Arduino UNO board, and hall effect sensor (7) Low voltage panel 23

Figure 4.5: Port crane (a) hoist motor reference speed profile (b) simulated vs. actual speed (c) non-optimal trajectory (d) simulated vs. actual power consumption 25

Figure 5.1: Port crane hoist and trolley mechanisms layout, (a) port crane motions, hoisting (1&4), lowering (6&3) and trolley (2&5) (b), port crane trajectories and constraints (c), and optimal port crane trajectory (d) 27

Figure 5.2: Port crane multiple optimal cycloid load trajectories 33

Figure 5.3: Real-world crane loading frequency per ship size [52] 37

Figure 5.4: Optimal vs. non-optimal crane trajectories, (a) crane productivity curve-based comparison (b) trajectory-based comparison 38

Figure 5.5: Simulation results, (a) A set of pareto optimal solutions (b) Optimal power consumption trajectories (c) Comparing optimal and non-optimal crane trajectories power consumption (d) Comparing optimal and non-optimal crane trajectories energy consumptio 39

Figure 6.1: EMR model of the port crane and its inversion-based local control system 42

Figure 6.2: Reduced port crane EMR model used for EMS development 44

Figure 6.3: Port crane EMR model used for PMP strategy development 44

Figure 6.4: PMP-based EMS for power split management in the batt-SC H-ESS 51

Figure 6.5: H-ESS reduction to an equivalent ESS given the battery's dominant capacitance 52

Figure 6.6: Ragone Plot showing the ESS power and energy densities [53] 53

Figure 6.7: Reduced port crane EMR model showing the filtering strategy development implementation 54

Figure 6.8: Implementation of the filtering strategy to manage the power split between the grid and the H-ESS 54

Figure 6.9: Step-by-step implementation of the combined EMS comprising of the filtering and the PMP-based sub-EMSs 55

Figure 6.10: Port crane energy consumption for one load cycle 56

Figure 6.11: Port crane simulated power consumption 57

Figure 6.12: One load cycle battery and supercapacitor SOCs 57

FIGURE 7.1: REDUCED PORT CRANE EMR MODEL 59
FIGURE 7.2: SUPERCAPACITOR PACK EQUIVALENT CIRCUIT [62] 60
FIGURE 7.3: BATTERY PACK EQUIVALENT CIRCUIT [62] 61
FIGURE 7.4: GENERALISED PORT CRANE H-ESS SIZING FRAMEWORK 62
FIGURE 7.5: OPTIMAL BATTERY AND SUPERCAPACITOR CURRENTS 66
FIGURE 7.6: SUPERCAPACITOR SIZE VS. H-ESS COST 67
FIGURE 7.7: BATTERY SIZE VS. H-ESS COST 68
FIGURE 7.8: PSO H-ESS COST CONVERGENCE PLOT 68

List of Tables

TABLE 3.1: GAPS IN LITERATURE 8
TABLE 4.1: PORT CRANE MAIN PARAMETERS 17
TABLE 4.2: PORT CRANE MATHEMATICAL MODELLING EQUATIONS 20
TABLE 4.3: MODELLING THE PORT CRANE LOCAL CONTROL SYSTEM 22
TABLE 5.1: OPTIMAL TRAJECTORY LOAD CYCLE DURATION 37
TABLE 6.1: H-ESS PARAMETERS 41
TABLE 6.2: H-ESS MATHEMATICAL MODELLING EQUATIONS 43
TABLE 7.1: SUPERCAPACITOR MODULE AND BATTERY CELL PARAMETERS [62] 66
TABLE 7.2: SIMULATED BATTERY AND SUPERCAPACITOR SIZES 67

Nomenclature

$\boldsymbol{A}$	Shipping Container frontal area.
$\boldsymbol{C_x}$	Air density coefficient.
$\boldsymbol{f}$	Trolley wheels rolling resistance coeff.
$\boldsymbol{F_{env}}$	Total environmental resistance force.
$\boldsymbol{F_{load}}$	Crane hoisting force.
$\boldsymbol{F_{load_t}}$	Trolley traction force.
$\boldsymbol{g}$	Gravitational acceleration.
$\boldsymbol{i_{hoist}}$	Hoist drive current.
$\boldsymbol{i_{bat}}$	Battery current.
$\boldsymbol{i_{dc}}$	DC-bus current.
$\boldsymbol{i_{dc_bat}}$	Battery current after chopper.
$\boldsymbol{i_{dc_grid}}$	Grid current after inverter.
$\boldsymbol{i_{dc_sc}}$	Supercapacitor current after chopper.
$\boldsymbol{i_{grid}}$	Grid current.
$\boldsymbol{i_{hess}}$	H-ESS current.
$\boldsymbol{i_{Rb}}$	Braking resistor current.
$\boldsymbol{i_{sc}}$	Supercapacitor current.
$\boldsymbol{i_{source}}$	Summation of Grid and H-ESS current.
$\boldsymbol{i_{trac}}$	Traction system current.
$\boldsymbol{i_{trolley}}$	Trolley drive current.
$\boldsymbol{I_{GB}}$	Hoist gearbox ratio.
$\boldsymbol{I_{GB_t}}$	Trolley gearbox ratio.
$\boldsymbol{M_L}$	Mass of crane load.
$\boldsymbol{M_{L+tr}}$	Mass of crane load and trolley.
$\boldsymbol{R_{drum}}$	Cable drum radius.
$\boldsymbol{R_{wheel}}$	Trolley wheels radius.

T_m	Hoist drive torque.
T_{m_t}	Trolley drive torque.
T_{GB}	Gearbox torque.
U_{bat}	Battery voltage.
U_{dc}	DC-bus voltage.
U_{grid}	Grid voltage.
U_{sc}	Supercapacitor voltage.
V_{load}	Crane load hoisting velocity.
V_{tr}	Crane trolley velocity.
V_w	Wind speed.
η_{ED}	Hoist drive efficiency.
η_{ED_t}	Trolley drive efficiency.
η_{GB}	Hoist gearbox efficiency.
η_{GB_t}	Trolley gearbox efficiency.
ω_m	Hoist drive shaft rotational speed.
ω_{m_t}	Trolley drive shaft rotational speed.
ω_{drum}	Cable drum rotational speed.
ω_{wheel}	Rotational speed of trolley wheels.
ρ	Air density at sea level.
$_ref$	Subscript for a reference variable.

1. Introduction

This study focuses on transportation systems, specifically the energy management of port cranes. More than 80% of global trade is seaborne [1], with at least 50% transported in shipping containers; these containers are loaded and unloaded at ports using port cranes [2]. Figure 1.1 illustrates the context of this study with an overview of a container port terminal, which includes ships, port cranes, trucks, and smaller yard cranes. Port cranes, also known as ship-to-shore (STS) cranes, are the largest energy consumers within the port, accounting for up to 40% of the port's energy consumption [3]. Port cranes regenerate more than 50% of the energy used to lift containers when lowering them [2][4], and reusing this regenerative braking energy improves energy efficiency. The European Council has endorsed targets for European ports to achieve 30% energy efficiency and 27% renewable energy penetration by 2030 [3]. It is shown in [3] that peak energy consumption accounts for 25-30% of the port's monthly electricity bill; port cranes are the most significant contributors to peak energy consumption. As such, they are well-suited for peak-shaving to improve energy efficiency. Consequently, port cranes were selected as the subject of this study due to the significance of the port industry in global trade and the critical role of port cranes in port operations. Furthermore, they offer the greatest potential for improving energy efficiency, peak-shaving, and renewable energy penetration within the port.

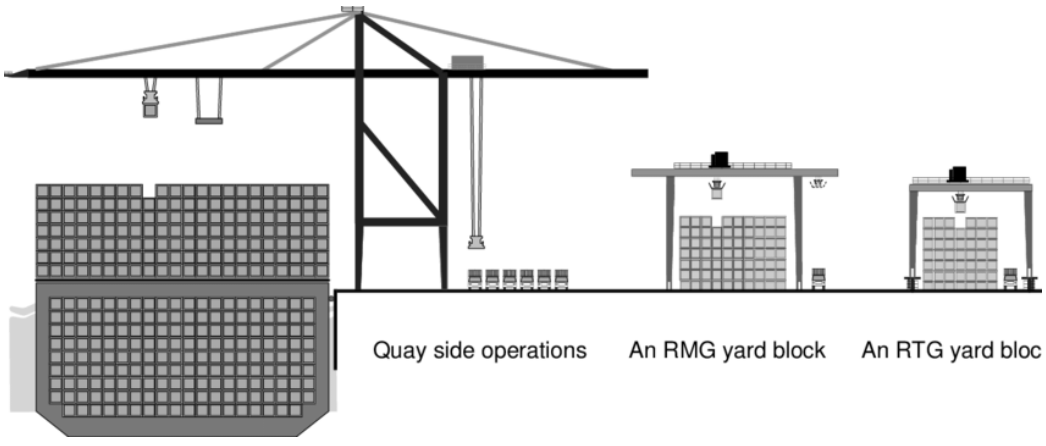


Figure 1.1: Port terminal overview

It has been shown that faster port cranes can reduce shipping vessel energy costs by up to 25% [3]. The reduction of the time ships spend in the port depends on the rate at which port cranes load/unload shipping containers; furthermore, this rate is used in the port industry to measure port productivity [5]. Full crane automation has been shown to result in faster crane loading speed and increased productivity [5]. Furthermore, [5] shows the desired trajectory of a crane transferring a container between ship and shore, noting that further research is required to develop an optimal trajectory for automated cranes. In [6], it is demonstrated that optimal trajectories for overhead cranes improve both productivity and energy efficiency. Given these research gaps, this study will develop an optimal trajectory for port cranes as a solution to the energy management problem for port cranes.

2. Background

2.1 Scientific Context of This Study

This study falls under efficient transportation systems with hybrid energy storage systems (H-ESS), as shown in Figure 2.1. There is a growing trend in the application of multiple energy sources and energy storage across various transportation systems, such as electric vehicles (EVs), trains, electric buses, elevators, and port cranes, leading to an increasing need for energy management strategies (EMSs) [7], [8], [9], [10]. The review in [3] highlights the rising number of research papers on energy efficiency in ports, however, significant research gaps remain to be addressed. The focus of this study is on EMSs for port cranes.

This study uses the energetic macroscopic representation (EMR) formalism [11] to develop the system model for the port crane, its local control system, and the EMS. This formalism has been widely used in EMS studies for transportation systems [12]. The study also includes the development of optimal trajectories as part of the EMSs, given its contribution to energy efficiency, as shown in [13]. Another key research area addressed in this study is energy storage and the reuse of regenerative braking energy [14].

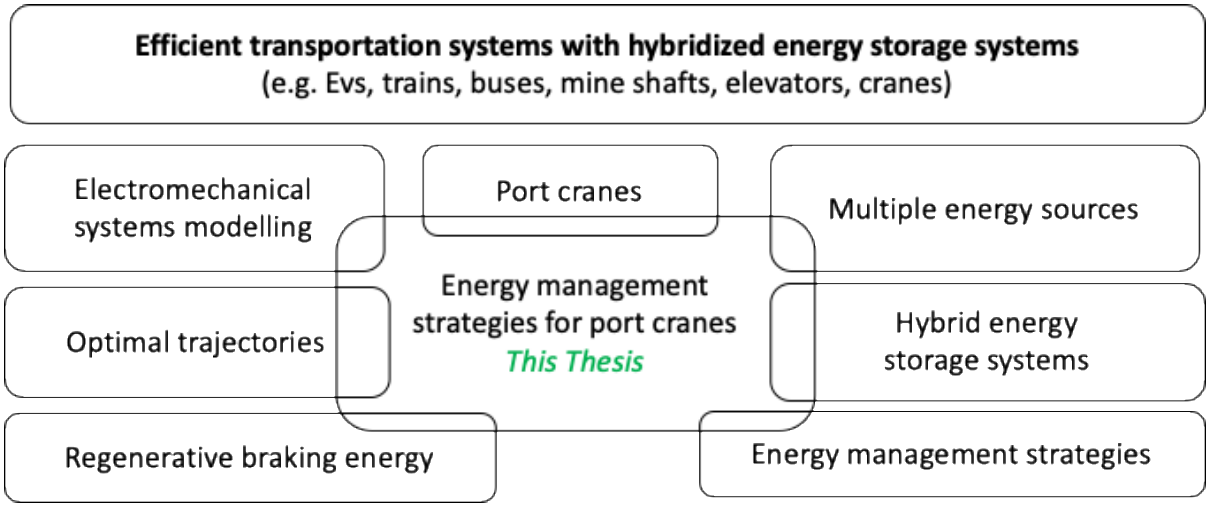


Figure 2.1: Scientific context of this study

2.2 Thesis Objective and Approach

2.2.1 Research Objectives

The main objective of this study is to develop an energy management strategy to reduce port crane energy consumption from the grid. The strategy combines two energy management techniques, which are:

- Optimal crane load handling trajectory
- Optimal energy management algorithm

The anticipated outcome of the two energy management techniques is to reduce both the crane's overall and dynamic energy consumption. The optimal energy management algorithm manages the storage and reuse of the crane's regenerative braking energy in the H-ESS.

2.2.2 Research Questions

This study aims to answer the following main research question:

1. What is the optimal energy management strategy for port cranes?

The main research question is further divided into the following sub-questions:

1.1. What is the optimal energy management algorithm for storage and reuse of regenerative braking energy for port cranes?
1.2. What is the optimal load handling trajectory for port cranes?

2.2.3 Methodology

This thesis aims to develop an energy management strategy that combines the optimal crane trajectory with an optimal energy management algorithm. The methodology of the thesis is shown in Figure 2.2. The approach uses the energetic macroscopic representation (EMR)

formalism to develop the port crane model used for simulations. EMR is a graphical tool for modelling, control, and energy management for complex multi-physical energetic systems. It organises the interaction between subsystems in terms of power flows, ensuring adherence to the principles of physical interaction and causality, thereby breaking down the studied system into naturally interconnected elements [15]. EMR is used for this study due to its proven suitability in similar studies as an effective tool for model organisation and control design of complex energy conversion systems [16]. The thesis methodology consists of six steps.

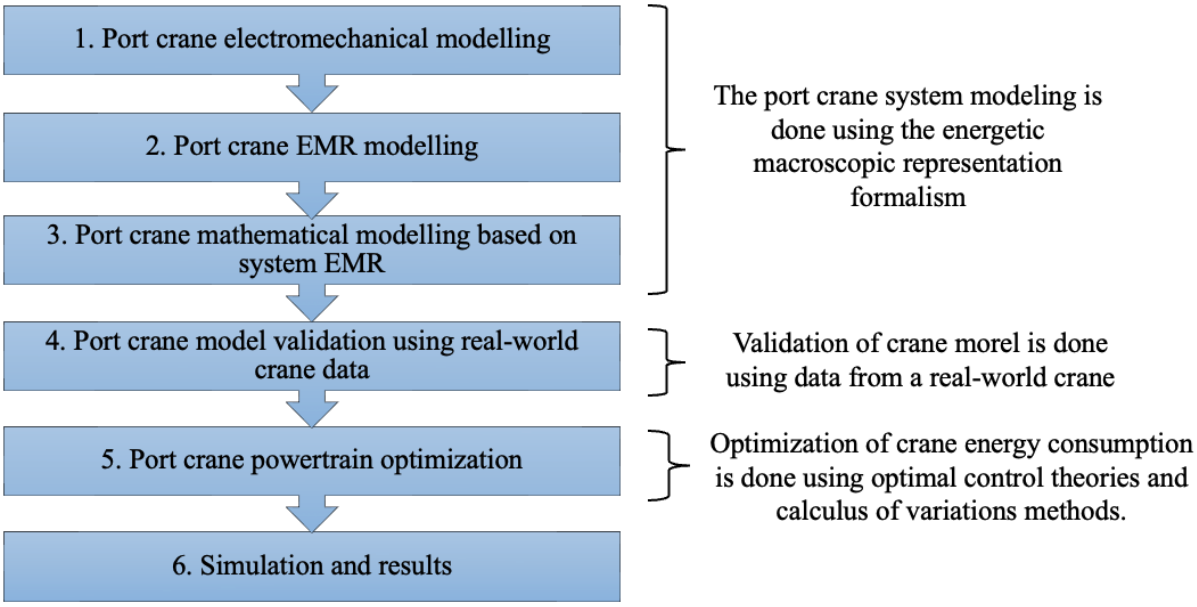


Figure 2.2: Thesis methodology

This thesis first develops the port crane's electromechanical system model. The system model is then transformed into an EMR-based model. Based on the EMR model, mathematical models are derived to develop the cranes' energy management algorithm. The system model will be tested and verified through MATLAB/Simulink simulations by comparing the system model results with actual crane data. Optimal control theories and calculus of variations methods are then applied to develop the port crane's energy management strategies. Finally, simulations for the optimal energy management strategy are performed in MATLAB/Simulink using the EMR library, and results are obtained.

2.3 Chapter Summary

This chapter provides the scientific context for energy management in efficient transportation systems with hybrid energy storage systems (H-ESS), specifically focusing on port cranes. It highlights the increasing adoption of multiple energy sources and storage systems in transportation sectors such as EVs, trains, buses, and elevators, emphasising the need for energy management strategies (EMSs).

Despite growing research in port energy efficiency, gaps remain in optimising crane energy consumption. This study employs the Energetic Macroscopic Representation (EMR) formalism to model port crane systems, local control mechanisms, and EMSs. The research objective is to develop an optimal energy management strategy that minimises port crane energy consumption from the grid. This is achieved through two key techniques: an optimal crane load handling trajectory and an optimal energy management algorithm for storing and reusing regenerative braking energy. Using MATLAB/Simulink simulations, the study applies optimal control theories and calculus of variations to refine energy management strategies, ensuring improved energy efficiency in port crane operations.

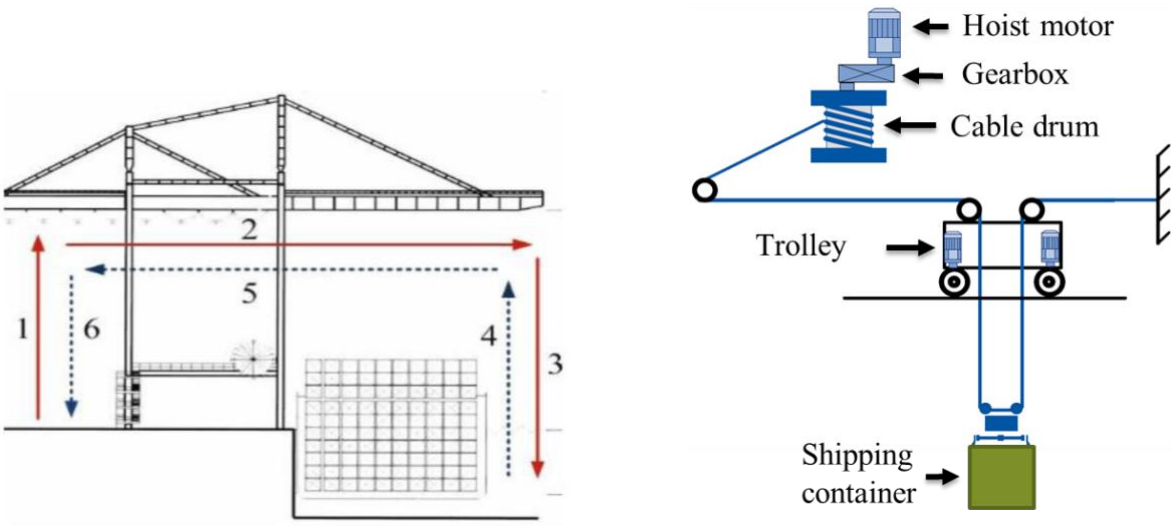
3. Literature Review

3.1 Literature Review

3.1.1 Studied Port Crane System

First, the port crane system model is presented to provide further context to the study. Figure 3.1 illustrates the details of the studied port crane system. Figure 3.1a shows the crane motions, which include lifting (1&4), trolley (2&5), and lowering (3&6). Port crane sizes vary according to the size of ships they can handle. There are three main port crane sizes: the Panamax crane, the Port Panamax crane and the Super Post Panamax crane [17].

Figure 3.1b shows the crane's drivetrain which consists of hoist motors, a gearbox, a cable drum, wire ropes, a spreader, a trolley, and trolley motors. Figure 3.2 shows the crane's powertrain which consists of the utility grid supply, rectifier, braking resistor, inverters and the crane load hoisting system/drivetrain. In this study, a battery-supercapacitor H-ESS is introduced to the port crane. The crane load consists of the standard 20 ft or 40 ft long shipping container [18], with a maximum gross weight of 30 480 kg.



(a) (b)

Figure 3.1: Port crane motions (a), port crane drivetrain (b)

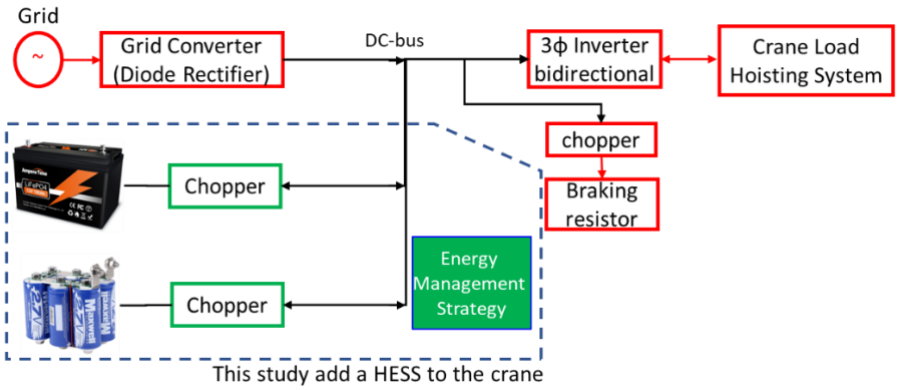


Figure 3.2: Port crane powertrain

3.1.2 Gaps in Literature

This section summarises the research gaps that this study addresses. The gaps in the literature are presented in Table 3.1.

Table 3.1: Gaps in literature

Research Area	Research Gaps	Key References
Port cranes	• Literature lacks studies that explain the economic contribution, viability, applicability and best practices regarding the use of clean and renewable energy for ports. • There are no detailed studies in energy management strategies for port cranes; previous research focuses on small yard cranes. • Automation of port cranes is in the early stages of implementation and dealing with the crane's dynamic behaviour is largely reliant on skilled crane drivers. • The contribution of crane automation to resolving the energy management problem has not been well studied.	[3], [17], and [19]

Research Area	Research Gaps	Key References
Hybrid energy storage systems and multiple energy sources	• Previous port crane studies mostly apply one ESS; this study includes a battery and supercapacitor ESS, along with a grid connection. • Previous studies focused on high power density ESS (supercapacitors & flywheels) for peak shaving and not on high energy density ESS (batteries). • There is therefore a need to develop a generalised energy storage sizing guideline for port cranes.	[14], [19], and [20]
EMR modelling of port cranes	• Modelling of port cranes using EMR formalisms has not been researched in the past. • Validation of EMR models using real-world data has not been done for port cranes. • The use of EMR formalism/models in hardware in the loop validation has not been done for port crane energy management strategies. • The use of the EMR formalism allows for a standardised and generalised approach to solving the energy management problem for port cranes. The EMR formalism provides a generalised methodology for system modelling, local control system development, and energy management strategy development. EMR formalism also provides a MATLAB/Simulink library for simulations and validation of the developed port crane system and its energy management strategy.	[15] and [12]

Research Area	Research Gaps	Key References
Energy management strategies for port cranes	• There are no previous studies that address the energy management problem for port cranes using an optimal load-handling trajectory. • Rule-based energy management strategies based on port crane operating modes have not been researched. • Optimisation-based energy management strategies for port cranes are in the early research stages. • One of the most advanced studies on port cranes is in [14], however, only optimal powertrain sizing is addressed and not energy management. • Previous optimal trajectory studies only consider the load sway problem and not a combination of horizontal and vertical movement of the load between ship and shore.	[12], [21], [22], [23], and [24]

3.2 Review of Energy Management Strategies

There has been a growing trend in the electrification of traction systems in port terminals to decrease energy consumption, increase energy efficiency, and support system decarbonisation [25]. A key aspect of electrifying traction systems is the application of energy storage systems such as batteries, supercapacitors (SCs), fuel cells, and flywheels [14], [25], [26]. When used individually, energy storage systems such as batteries and supercapacitors have limited power or energy density, but they are complementary when combined into a hybrid energy storage system (H-ESS) [26]. In addition to the energy storage systems listed above, traction applications such as port cranes regenerate energy during braking to slow the load down. The storage and reuse of regenerative braking energy can improve the crane's energy efficiency [25].

The use of multiple energy storage system (ESS) in a H-ESS requires an energy management strategy (EMS) to control the power split between the ESSs. EMSs are categorised into optimisation-based or rule-based type strategies [16] as shown in Figure 3.3.

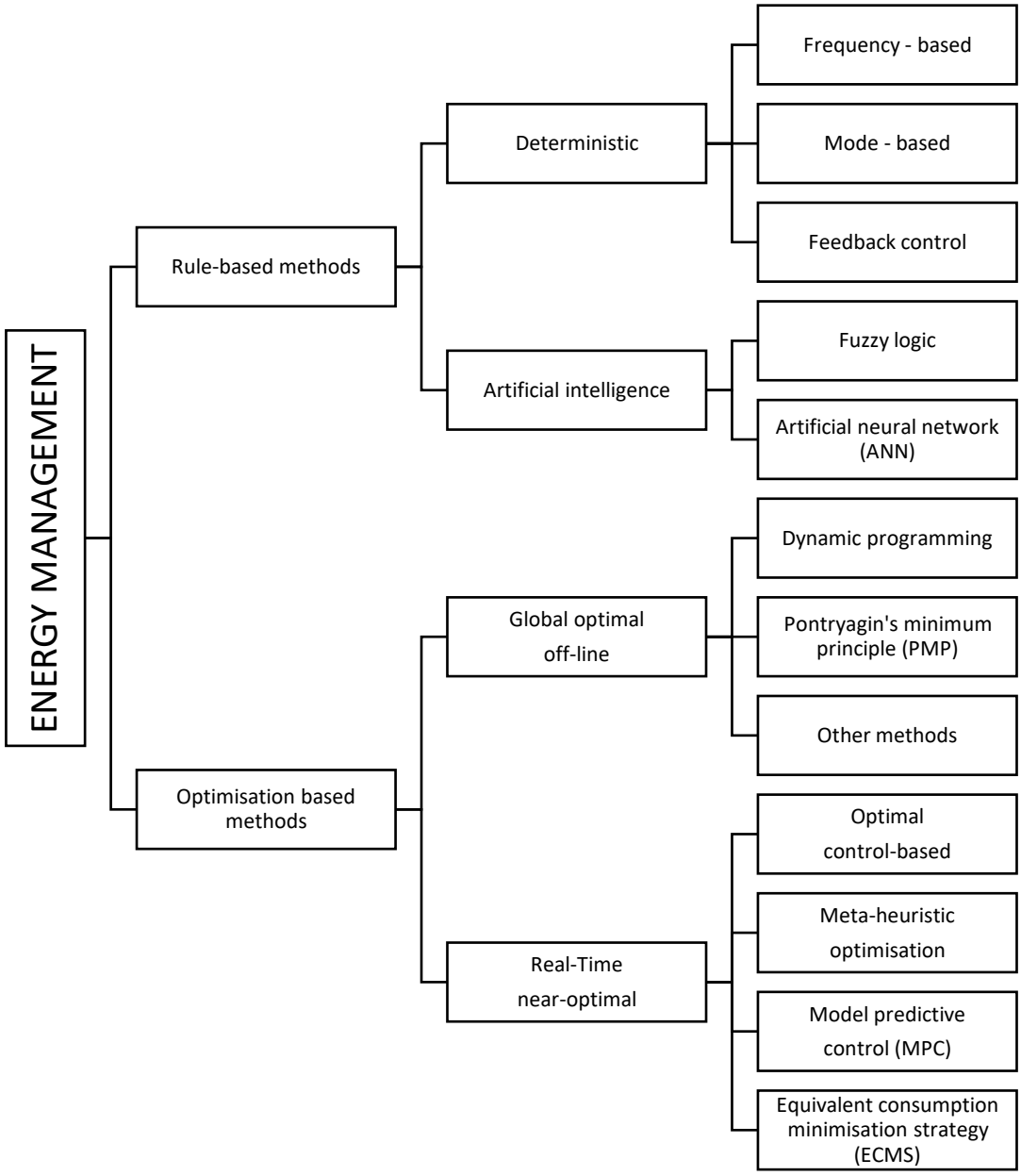


Figure 3.3: Classification of energy management methods [21]

Rule-based EMSs produce non-optimal results, whereas global optimal EMSs yield optimal results but are computationally costly and complex [12]. Research on EMS for port crane applications is in the early stages [27]. However, port cranes share the same type of electric powertrain as other well-researched transportation systems, such as electric vehicles (EVs),

electric buses, lifts, and electric trains [28]. A lack of optimisation-based EMS usage for port cranes is highlighted in [27], and studies in [29] and [30] have shown that rule-based EMSs, based on proportional-integral (PI) and set-point controllers, have been widely implemented for port cranes. In [31] a particle swarm optimisation (PSO) algorithm is used to size a supercapacitor energy storage system (ESS) with the aim of reducing crane peak power demand through storing and reusing regenerative braking energy. In [32] it is proposed that port cranes can become "near-zero energy load systems" by using regenerative energy (RE) stored in supercapacitors as the primary energy source, consuming minimal energy from the grid only for system losses and RE shortfall. However, this is not currently feasible due to the low energy density of SCs. It has been shown in [33] that ports can become "near-zero energy load systems" by using hydrogen energy storage systems resulting in up to a 51.8% reduction in their Levelized Cost of Energy. A port-level flywheel energy storage system is simulated in [34] for a group of port cranes to reduce the group's maximum power demand (peak shaving). The energy storage systems used in the studies above only include high-power density supercapacitors or flywheels, which achieve peak power shaving. However, they do not incorporate a high energy density device such as a battery, to achieve energy savings and efficiency by reusing regenerative braking energy.

In [14] a comprehensive HESS optimal sizing strategy is presented for hybrid rubber tyre gantry (RTG) crane with batteries and SCs as its two energy sources. However, the energy management problem is not addressed. It is shown that, compared with the traditional diesel engine RTG crane, the battery-SC hybrid RTG crane, has great potential for regenerative energy recovery, which leads to a reduction in fuel costs and carbon emissions. The RTG crane is smaller but handles the same size shipping containers as the ship-to-shore (STS) crane in this study. The findings in [14] confirm that a battery-SC HESS is potentially suitable for port crane applications. To the best of the author's knowledge, there are no studies on EMS development for port cranes powered by batteries-supercapacitors H-ESS and the grid. This represents a unique contribution of this work.

The main research on the development of optimal trajectories for port cranes is summarised by five overhead crane load handling trajectories in [13]. These five trajectories focus only on the horizontal trolley motion of the port crane and do not consider the effects of hoisting the load. The trajectories show that overhead cranes generally have an initial acceleration period,

followed by a period of constant velocity, and finally, a deceleration period when the load reaches its destination. The crane motions described results in a trapezoidal shaped non-optimal trajectory. Therefore, this study develops an optimal crane load handling trajectory that considers both horizontal and vertical crane load motions. Further research on trajectory development for other types of cranes, other than port cranes, is shown in [35] and [36]. The development of the optimal load handling trajectory for port cranes intuitively leads to automation, which is necessary to eliminate human error in port crane load handling motions. Advancements in port crane automation, for both horizontal and vertical motions are shown in [17]. The review in [17] shows that port crane productivity is directly related to the time it takes to transfer the shipping container between ship and shore. Therefore, the optimal trajectory for port cranes to be developed in this study will consider crane automation to minimise load handling time. The study in [23] evaluates fast trajectories for handling port crane loads; however, this study uses a non-optimal trajectory.

The most advanced studies on powertrain optimisation for traction applications are for electric vehicles (EVs). These studies solve the energy management problem using various rule-based and optimisation-based methods, including dynamic programming (DP) algorithms, filtration-based controllers (FBC), model predictive controllers (MPC), rule-based controllers (RBC), fuzzy logic controllers (FLC), Pontryagin's minimum principle (PMP), and particle swarm optimisation (PSO) algorithms [37],[38],[39]. Advanced research conducted on EV applications, therefore, highlights the existing gaps in energy management systems (EMSs) and hybridisation of ESSs for port crane applications.

The studies mentioned above have developed solutions to the energy management challenge in electric vehicle powertrains, utilising computational techniques including optimisation and rule-based algorithms. Unlike EV applications, port cranes have a utility grid connection in addition to the H-ESS in their powertrain. Port cranes also have a different power demand profile to that of EVs. This study aims to develop an optimal EMS for port cranes, combining optimisation-based Potryagin’s Minimum Principle (PMP), rule-based filtering EMS development approaches, and the crane’s optimal load handling trajectory. Studies in [40] and [12] show that PMP produces global optimal results close to those of DP, which is the benchmark for global optimisation strategies. PMP has also been demonstrated to save up to 77% of computational time compared to DP [40]. Furthermore, PMP produces analytical

solutions that are easier to implement [40] whereas DP requires special software toolboxes [41]. The selection of PMP for this study is based on these advantages. Conversely, the rule-based EMS was selected because it is categorised under the most classical EMSs and produces near-optimal results, as shown in [12]. To the best of the author's knowledge, there are no studies on port cranes where the energy management problem is solved by using a combination of optimisation algorithms and the crane's optimal load-handling trajectory.

Furthermore, studying port cranes requires an appropriate system modelling technique. Port cranes can be classified under multi-converter multi-machine systems as described in [42]. It has been shown in [42] and [15] that the graphical Energetic Macroscopic Representation (EMR) formalism can be used to model multi-converter multi-machine systems. The EMR formalism is used to develop system models, local control, and EMS for complex multi-physical energetic systems [15]. EMR is a divide-and-conquer approach to system modelling that represents subsystem interaction using power flows whilst respecting the three principles of integral causality, interaction, and inversion [12]. Integral causality means that the output to the energetic system is a functional integral of the input; the interaction principle means that subsystems interact using action and reaction variables and the product of the variables is the instantaneous power exchange between subsystems; lastly, the inversion principle applies direct and indirect mathematic inversion of each subsystem to develop the system's local control scheme [15]. To the best of the author's knowledge, there are no studies on the development of EMR-based port crane models.

3.3 Chapter Summary

The literature review explores the growing trend of electrification and hybrid energy storage systems (H-ESS) in port terminals, emphasising the need for energy management strategies (EMSs) to improve efficiency. It highlights that while rule-based EMSs are commonly used for port cranes, they are non-optimal, whereas optimisation-based methods provide superior results but are computationally demanding. The study identifies a research gap in port crane EMSs, as existing studies primarily focus on electric vehicles (EVs), buses, and trains. Several approaches to energy recovery, such as regenerative braking storage in supercapacitors (SCs) and flywheels, have been explored, but lack integration with high-energy-density batteries for optimal efficiency.

The review also discusses optimal load handling trajectories, which improve automation and reduce energy consumption, yet most existing methods neglect vertical load motion. Additionally, it evaluates optimisation algorithms such as Pontryagin's Minimum Principle (PMP), which balances computational efficiency with near-global optimal results. The Energetic Macroscopic Representation (EMR) formalism is identified as a promising system modelling technique for multi-converter, multi-machine systems, though its application to port cranes remains unexplored. This study aims to bridge these gaps by developing an EMS that integrates optimisation techniques, load handling trajectory optimisation, and EMR-based system modelling to enhance port crane energy consumption.

4. Port Crane System Modelling

4.1 Port Crane Electromechanical System Description

Figure 4.1 illustrates the studied port crane system, focusing on the load-handling mechanism of a ship-to-shore (STS) crane, which is the largest type of port crane. Currently, most port cranes operate with a grid connection as their sole energy source. A three-phase AC/DC bi-directional inverter links the DC bus to the crane motors, which provide the energy for lifting and moving loads through the hoisting and trolley systems. These systems include components such as gearboxes, drums, ropes, pulleys, and spreaders.

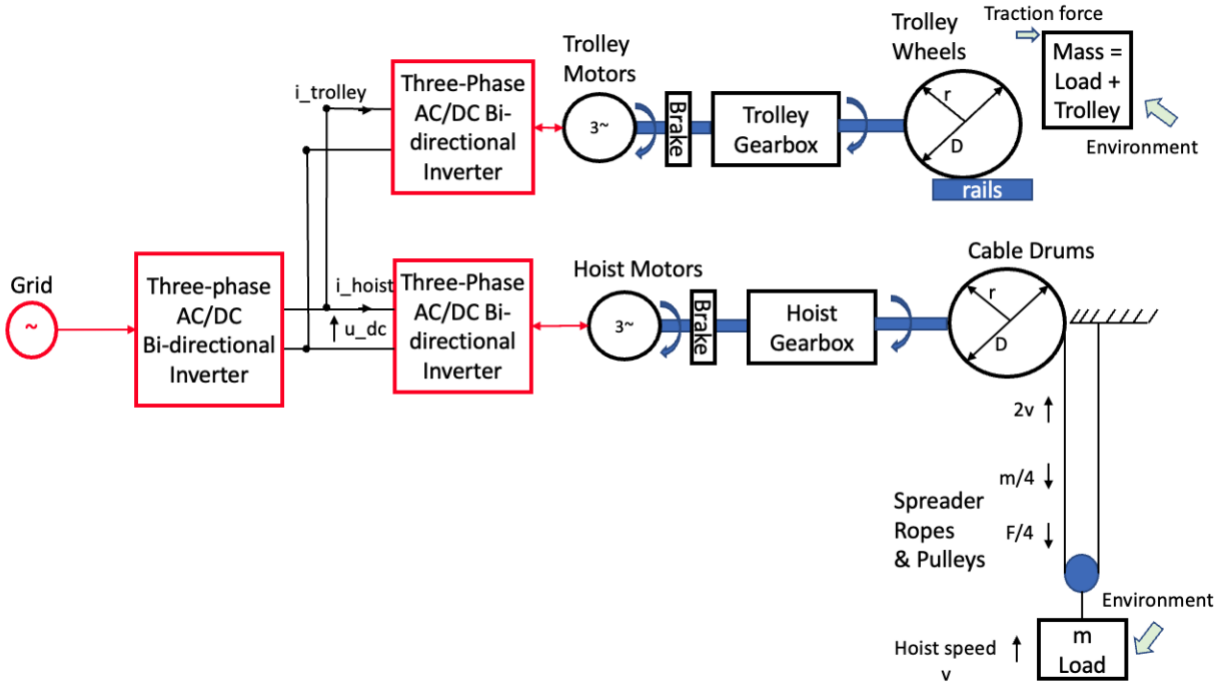


Figure 4.1: Studied port crane system

The load-handling mechanism encompasses all the mechanical dynamics of the crane, while external factors like braking, gravitational, and wind forces impact the container load. This crane model was developed with an emphasis on energy management. To transport the load between the ship and the shore, the hoisting system generates vertical lifting force, and the trolley system produces horizontal force. Table 4.1 provides the parameters of a real-world port

crane located at the Cape Town Container Terminal in South Africa, which was utilised for MATLAB-Simulink simulations in this research. The crane is capable of handling loads up to 65 tons, with lifting heights reaching 57 meters on the landside and 73 meters aboard shipping vessels. Its energy is supplied by a 1.6 MVA on-board three-phase transformer that steps down an 11 kV grid input to 650 V.

The crane achieves hoist speeds of 90 meters per minute when loaded and 180 meters per minute when unloaded, with acceleration taking approximately 2.5 seconds and steady-state operation lasting around 15 seconds. Typically, a port crane demands between 1 MW and 2 MW of power, consuming 8 to 16 kWh per 30-second load cycle while regenerating 5 to 10 kWh per cycle. In real-world operation, the crane dissipates most of the regenerated energy from its hoist motors through a braking resistor on the DC bus. The crane has bi-directional inverters, which allow it to redirect the regenerated energy back to the grid or auxiliary systems, like the cabin air conditioner. Operating 24 hours a day and processing an average of 30 containers per hour [20], a port crane uses around 17 MWh daily, equating to roughly 6 GWh annually.

Table 4.1: Port crane main parameters

Hoist System Parameters	
Load mass	65 t with shipping container 18 t empty spreader
Hoisting Speed	1.5 m/s full-load speed 3 m/s no-load speed
Electric drive	2 x 500 kW induction machines Efficiency 90%
Gearbox	Ratio 21.389 Efficiency 85%
Cable drum diameter	1.365 m
Trolley System Parameters	
Trolley Speed	3.83 m/s - maximum
Electric drive	4 x 55 kW induction machines Efficiency 90%
Gearbox	Ratio 21.389 Efficiency 85%
Trolley wheels diameter	710 mm
Coefficient of friction rail-to-wheel	0.02

4.2 Port Crane Energetic Macroscopic Representation

Figure 4.2 illustrates the EMR-based model of the port crane system, including the local control and energy management strategy (EMS). The EMR formalism enables the decoupling of the crane's mathematical model into distinct layers for the EMS and local control systems. The EMS operates at a supervisory level, positioned above the local control layer, with each layer requiring separate treatment due to differences in their dynamics. While dynamic models are used for the load and DC-bus capacitor, static models represent the other components of the port crane. This approach is justified, as faster dynamic subsystems can be simplified into equivalent static models by assuming perfect control with instantaneous responses to input references, as demonstrated in [43] and [44].

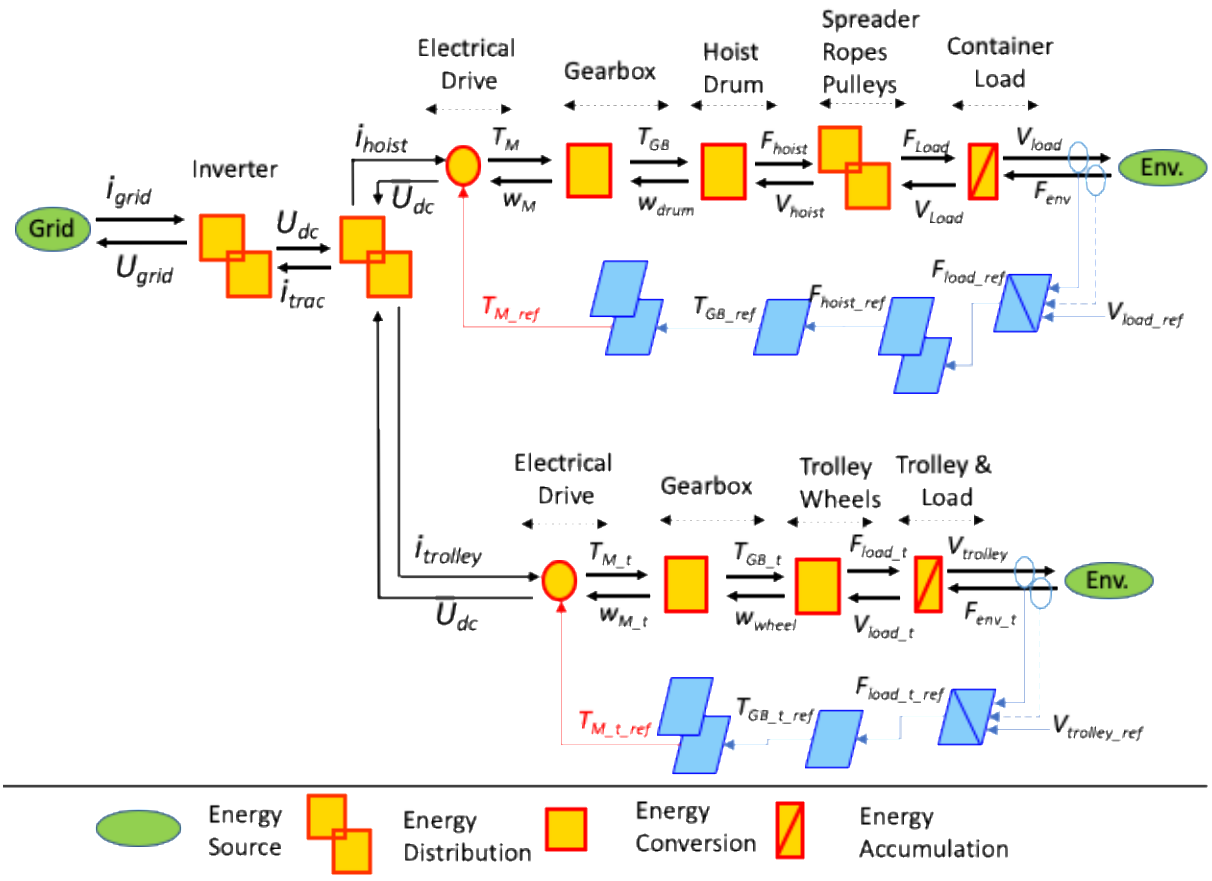


Figure 4.2: Port crane EMR and inversion-based local control

4.3 Port Crane Mathematical Modelling

Table 4.2 outlines the equations used to represent the port crane model depicted in Figure 4.2. The mathematical model for electric vehicles (EV) from [12] serves as the foundation for developing the port crane model, due to the drivetrain similarities between the two systems. The electrical drive introduces the current i_{trac} in equation (4.3), which is processed by the induction machine to generate the output torque T_{GB} as expressed in equation (4.4). The gearbox dynamics, including the input speed ω_m, output speed ω_{drum}, and torque T_{GB} , are described by equations (4.4) and (4.5). Rotational motion in the cable drum is converted to linear motion in the hoist ropes through equations (4.6) and (4.7). The hoisting speed V_{hoist} and force F_{hoist} in the hoist wires are modelled using equations (4.8) and (4.9). The hoisting speed of the container, V_{Load}, is defined in equation (4.8). Similarly, equations (4.13) through (4.18) describe the crane trolley system's electrical drive, gearbox, trolley wheel, and load dynamics in a manner analogous to the crane hoisting system outlined in equations (4.1) to (4.11). All equations are presented in scalar form, as this study primarily focuses on energy management.

4.4 System Disturbances

The total force, F_L , required by the crane to lift the load is described in equation (4.10). The frictional force, F_{res}, between the cable drum and the wire ropes is considered negligible due to the significant 65-ton load, which exerts a gravitational force of 637 kN. Equation (4.12) quantifies the gravitational and air drag resistance forces acting on the shipping container. The environmental forces affecting the trolley and hoist loads, as expressed in equations (4.12) and (4.19), include rolling resistance, gravitational forces, air drag, and wind forces. Among these, wind, rolling resistance, and air drag are identified as the primary disturbances in the crane's load-handling process. This study specifically accounts for the influence of wind on the crane load, assuming it acts in the direction of the trolley's movement between the ship and the shore.

Table 4.2: Port crane mathematical modelling equations

	Hoist System Modelling	
Electrical Drive	$M_{@motor_shaft} = M_{Load}/4$	(4.1)
	$T_m = T_{m_ref}$	(4.2)
	$i_{trac} = \frac{(T_m \omega_m)}{2(U_{dc}\eta_{ed}^{\gamma})} \begin{cases} \gamma = 1 & T_m\omega_m \geq 0 \\ \gamma = -1 & T_m\omega_m < 0 \end{cases}$	(4.3)
Gearbox	$T_{GB} = \frac{(T_m i_{gb})}{\eta_{gb}^{\gamma}} \begin{cases} \gamma = 1 & T_m\omega_m \geq 0 \\ \gamma = -1 & T_m\omega_m < 0 \end{cases}$	(4.4)
	$\omega_m = I_{gb} \times \omega_{drum}$	(4.5)
Cable drum	$\omega_{drum} = 4V_L/Dia_{drum}$	(4.6)
	$F_{hoist} = T_{GB}/R_{drum}$	(4.7)
Spreader System	$V_{Load} = V_{hoist}/2$	(4.8)
	$F_{Load} = 4F_{hoist}$	(4.9)
Load	$F_{Load} = M_L \frac{d}{dt} V_{Load} + F_{env}$	(4.10)
	$M_L = M_L/4$	(4.11)
Environment	$F_{env} = M_L g + 0.5\rho c_x A(V_L + V_w)^2$	(4.12)
	Trolley System Modelling	
Electrical Drive	$i_{trolley} = \frac{(T_{m_t}\omega_{m_t})}{2(U_{dc}\eta_{ed_t}^{\gamma})} \begin{cases} \gamma = 1 & T_{m_t}\omega_{m_t} \geq 0 \\ \gamma = -1 & T_{m_t}\omega_{m_t} < 0 \end{cases}$	(4.13)
Gearbox	$T_{GB_t} = \frac{(T_{M_t} i_{GB_t})}{\eta_{GB_t}^{\gamma}} \begin{cases} \gamma = 1 & T_{m_t}\omega_{m_t} \geq 0 \\ \gamma = -1 & T_{m_t}\omega_{m_t} < 0 \end{cases}$	(4.14)
	$\omega_{m_t} = I_{GB_t} \times \omega_{wheel}$	(4.15)
Trolley Wheels	$w_{wheel} = V_{trolley}/R_{wheel}$	(4.16)
	$F_{wheel} = T_{GB_t}/R_{wheel}$	(4.17)
Load	$F_{Load_t} = M_{L+tr} \frac{d}{dt} V_{trolley} + F_{env_t}$	(4.18)
Environment	$F_{env_tr} = M_{L+tr}(g + fg) + 0.5\rho c_x A(V_{tr} + V_w)^2$	(4.19)

4.5 Port Crane Local Control System

The EMR-based local control system for the traction component of the crane is depicted in the blue blocks of Figure 4.3. The EMR formalism is utilised to determine the tuning and control pathways necessary for developing the traction system's local control scheme, as illustrated in Figure 4.3. In this context, a tuning path links the tuning variable to the objective variable, which is the parameter being controlled [26]. The control path mirrors the tuning path. For this study, the tuning path begins with the tuning variable, which is the electrical drive torque (T_{m_ref}), and progresses to the control variable, which is the load speed (V_{Load}). The local control system for the crane hoist system is then methodically derived by inverting each subsystem, as explained in [45].

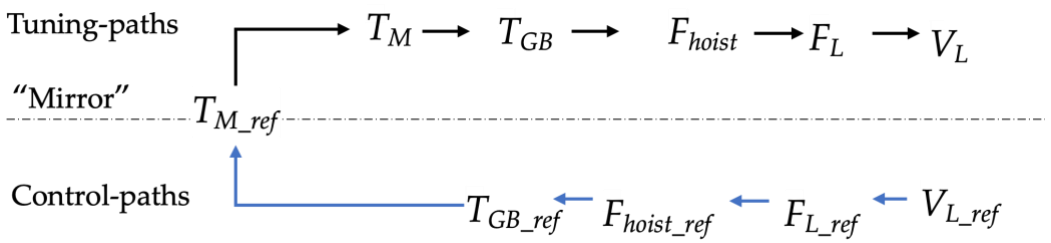


Figure 4.3: Port crane local control system

Similarly, the local control system for the crane trolley system is derived by following the tuning path from the tuning variable $T_{m_t_ref}$ to the control variable V_{Load_t}. Table 4.3 lists the mathematical equations used to model the port crane control system. For all mechanical transmission components except the load, the local control system is derived through direct inversion of the corresponding mathematical equations, as shown in equations (4.20) to (4.22), (4.24), and (4.25). For the load, an indirect inversion approach is applied, as modelled in equations (4.23) and (4.26). This involves a closed-loop proportional-integral (PI) controller, $C_{load}(s)$, which operates in a feedback loop. The PI controller produces the output F_{L_ref}, while its inputs include the measured load speed V_L, the disturbance F_{res}, and a reference hoist speed profile V_{L_ref}.

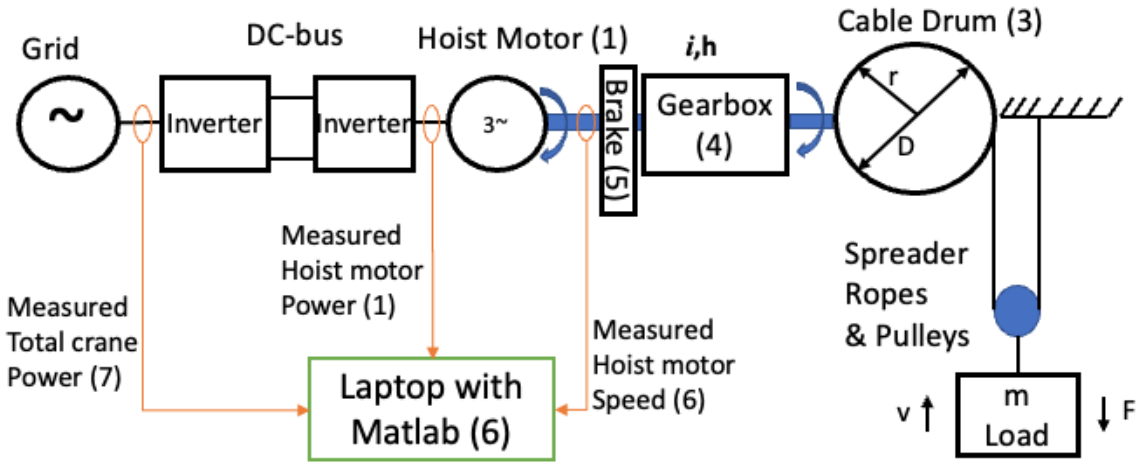
Table 4.3: Modelling the port crane local control system

Hoist Local Control System		
Gearbox	$T_{m_ref} = \frac{T_{GB_ref}}{i_{gb}\eta_{gb}^{\gamma}} \begin{cases} \gamma = 1 & T_m\omega_m \geq 0 \\ \gamma = -1 & T_m\omega_m \geq 0 \end{cases}$	(4.20)
Cable drum	$T_{GB_ref} = F_{hoist_ref} \times r_{drum}$	(4.21)
Spreader	$F_{hoist_ref} = F_{L_ref}/4$	(4.22)
Load	$F_{L_ref} = C_{load}(s)(V_{L_ref} - V_L) + F_{res}$	(4.23)
Trolley Local Control System		
Gearbox	$T_{m_t_ref} = \frac{T_{GB_t_ref}}{i_{gb_t}\eta_{gb_t}^{\gamma}} \begin{cases} \gamma = 1 & T_{m_t}\omega_{m_t} \geq 0 \\ \gamma = -1 & T_{m_t}\omega_{m_t} \geq 0 \end{cases}$	(4.24)
Wheel	$T_{GB_t_ref} = F_{load_t_ref} \times R_{wheel}$	(4.25)
Load	$F_{L_ref} = C_{load}(s)(V_{L_ref} - V_L) + F_{res}$	(4.26)

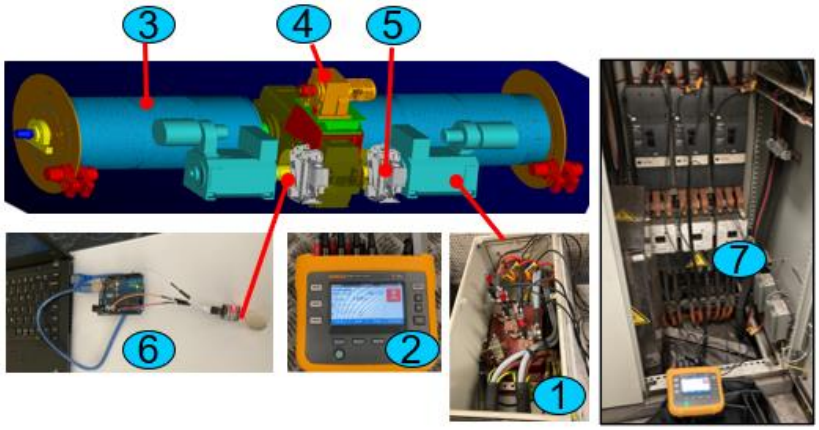
4.6 Port Crane System Model Experimental Validation

4.6.1 Experimental Setup

The validation of the crane's EMR model was performed using power consumption and hoist motor speed data collected from an actual STS crane at the Cape Town Container Terminal. The experimental setup, depicted in Figure 4.4, utilised a Fluke 1736 power logger to measure the crane's power consumption during container loading and unloading operations. Power data was recorded at the 500 kW hoist motors, which are the primary consumers of energy, and at the low-voltage (LV) panel supplying the crane. A Hall effect sensor, mounted near a magnet on the hoist motor shaft, captured the motor shaft speed. The sensor output was processed using an Arduino Uno board and a laptop running MATLAB/Simulink. During the experiment, the crane handled a 20-ton load.



(a)



(b)

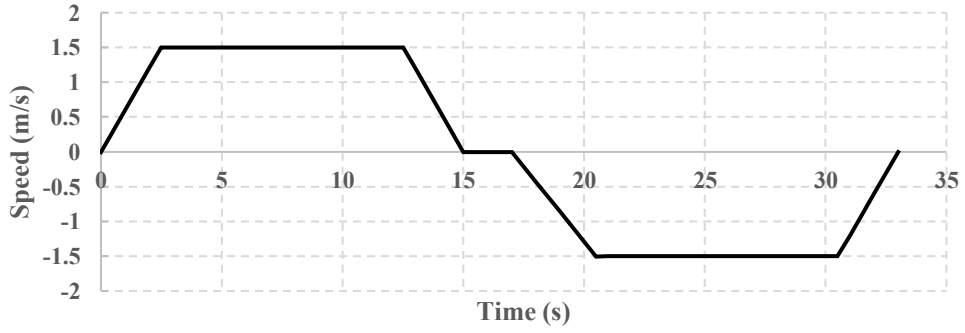
Figure 4.4: Experimental setup (a) and (b)**:** (1) Hoist motor (2) Fluke 1736 power logger (3) Cable drum (4) Gearbox (5) Mechanical brakes (6) PC, Arduino UNO board, and hall effect sensor (7) Low voltage panel

Real-world cranes are operated according to a predefined speed reference curve, as shown in Figure 4.5a. This trapezoidal-shaped speed profile includes an initial acceleration phase for lifting the load, a constant-speed phase, and a deceleration phase upon approaching the destination. The final stage involves lowering the load into its designated position, during which the hoist motors generate regenerative braking energy that is dissipated in the braking resistor. The use of this trapezoidal speed setpoint curve for the crane motors results in a non-optimal, trapezoidal power consumption trajectory. For validation purposes, the recorded motor speed from the real crane was used as the input speed (V_{Load_ref}) in the MATLAB/Simulink simulation. The simulated hoist motor power consumption was then compared with the actual power consumption data recorded from the crane.

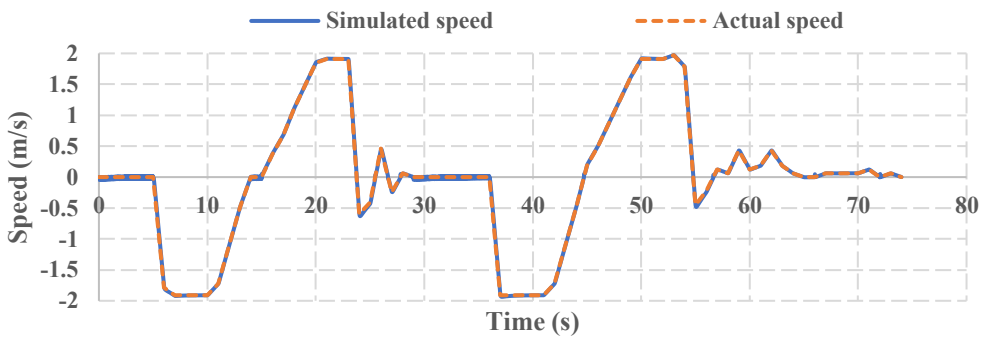
4.6.2 Experimental Results

Figure 4.5b demonstrates that the simulated load hoisting speed corresponds to that of the real-world crane. Figure 4.5c illustrates the load hoisting trajectory, which is non-optimal due to the trapezoidal-shaped reference speed curve. This trajectory was derived from the real-world speed data, but it is inverted since the load-handling spreader was initially suspended at height when the crane started operating—a typical resting position for crane operators.

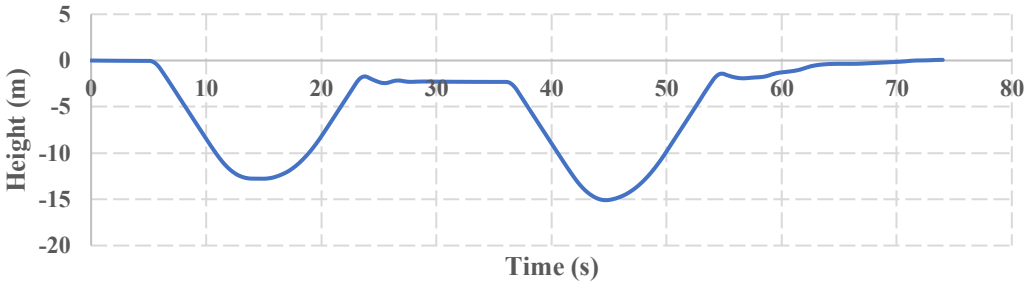
Figure 4.5d indicates that the power consumption curve from the crane's EMR simulation model closely aligns with that of the real-world crane. However, the real-world power consumption curve exhibits greater dynamical variations compared to the simulation. Studies in [43] and [44] validate the use of static models for fast dynamical crane components in energy management studies, as energy management strategies operate above the crane's control system, which demands fast dynamic responses. The highly dynamic nature of the real-world crane's power consumption curve is attributed to human operators and the crane's control system. To minimise these dynamical variations, automation of port cranes and the implementation of optimal sinusoidal speed setpoint curves are proposed. Based on these findings, it is confirmed that the EMR-based simulation model accurately reflects the actual crane's power consumption.



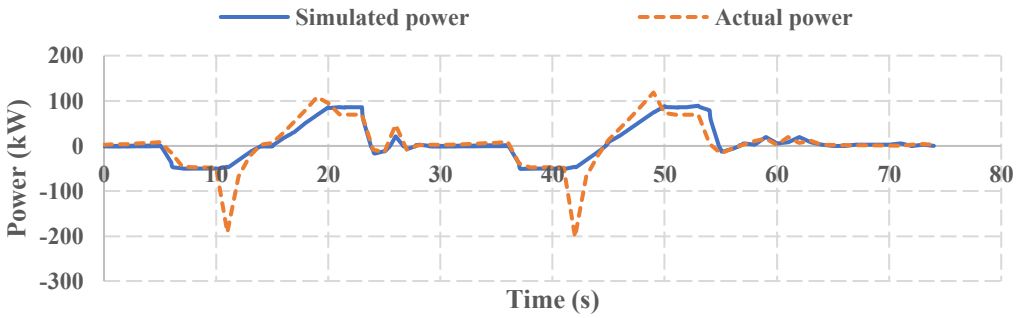
(a)



(b)



(c)



(d)

Figure 4.5: Port crane (a) hoist motor reference speed profile (b) simulated vs. actual speed (c) non-optimal trajectory (d) simulated vs. actual power consumption

4.7 Chapter Summary

This chapter used the EMR formalism to develop the port crane system model, which consists of the crane's EMR model, its local control system, and the mathematical equations governing the energy flow between the crane's subsystems. The crane's EMR model was validated using real-world crane data, confirming its accuracy in reflecting the actual crane's power consumption.

5. Development of The Optimal Port Crane Trajectory

This chapter focuses on developing an optimal load-handling trajectory for port cranes with the objective of minimising load cycle time and reducing energy consumption. The port crane EMR-based system model developed in Chapter 4 is used for simulations. The particle swarm optimisation algorithm is used to determine the set of Pareto optimal crane trajectories, taking into account variations in crane size, ship size, and wind speed.

5.1 Description of The Port Crane Load Handling Mechanism

Figure 5.1a illustrates the load-handling mechanism of the port crane, which comprises the load hoisting system and the trolley. When handling shipping container loads, the crane performs two main motions, as shown in Figure 5.1b: the horizontal trolley motion and the vertical hoisting and lowering motions. Additionally, the crane can execute a gantry motion, which involves moving sideways along the ship. However, this motion is performed without a load and does not involve the trolley, hoisting, or lowering motions. Therefore, the load-handling trajectory of the port crane primarily includes the trolley and hoisting motions. As depicted in Figure 5.1a, the load is suspended beneath the trolley, which moves back and forth between the ship and the shore. Steel wire ropes are employed to hoist and lower the load beneath the trolley, which is attached to the crane's spreader. The combination of the hoisting and trolley motions defines the path along which the load is transported between the ship and the shore.

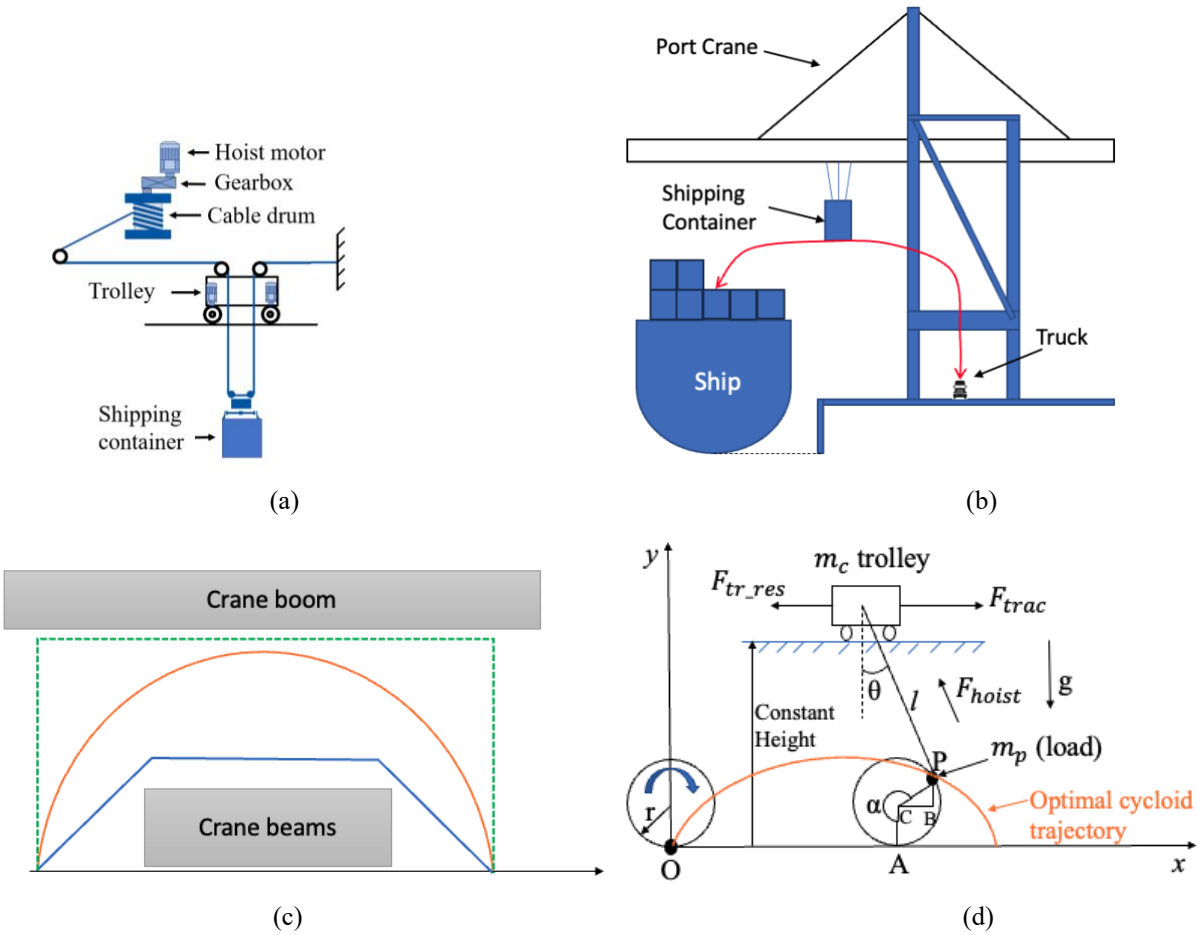


Figure 5.1: Port crane hoist and trolley mechanisms layout, (a) port crane motions, hoisting (1&4), lowering (6&3) and trolley (2&5) (b), port crane trajectories and constraints (c), and optimal port crane trajectory (d)

5.2 Optimal Port Crane Trajectory

The hoisting motions and mechanism of the crane, depicted in Figure 5.1b, are represented by three potential trajectories in Figure 5.1c. These trajectories, along with any paths in between, define the space within which the crane's optimal trajectory lies. The crane's load movement is constrained by the physical limits of the boom and bottom structure as it transfers containers between the ship and the shore. Port productivity is typically measured by the number of containers a crane handles per hour, referred to as moves per hour [17]. Therefore, the optimal trajectory for the crane is the one that minimises the time required to move a container between the ship and the shore.

The problem of determining the optimal trajectory for the port crane is analogous to a combination of the cart-pendulum and brachistochrone problems, both of which can be approached using Lagrangian mechanics. The brachistochrone problem, first solved in the 1600s by Bernoulli, Newton, and others [46], involves finding the fastest path for a bead to travel along a frictionless wire between two points under the influence of gravity. In the case of the port crane, the brachistochrone curve is inverted, and the forces acting on the load result from both gravitational forces and the crane motor's acceleration forces. The brachistochrone curve, a segment of a cycloid, represents the fastest path. For the port crane, the load (as analogous to the bead) follows this cycloidal trajectory for optimal travel between the ship and the shore, as shown in Figure 5.1d.

In [47], it is demonstrated that the brachistochrone curve adheres to the principle of stationary action, which also applies to the port crane's motion since it starts and ends at stationary points. Figure 5.1d presents a classical mechanics model of the port crane. The cart-pendulum representation is used for the trolley and suspended load, which is useful for addressing the load sway problem. However, this study does not focus on load sway which has been well researched [48], and is typically minimal in practice due to anti-sway control systems and the significant weight of the crane load, resulting in a very small θ.

Thus, the optimal trajectory for the crane is determined by solving the brachistochrone problem. This problem involves determining the shape of the curve along which a bead, starting from rest and influenced only by gravitational acceleration, travels between two points, $P_1$and P_2, in the shortest possible time without the influence of friction. The time required to travel between these two points is represented by the integral:

$$t_{12} = \int_{P_2}^{P_1} \frac{ds}{v} \tag{5.1}$$

Here, s represents the arc length, and v denotes the speed. The speed at any point along the curve is determined using the principle of conservation of energy, equating the kinetic energy to the gravitational potential energy as follows:

$$\frac{1}{2}mv^2 = mgy \tag{5.2}$$

Which gives:

$$\mathrm{v} = \sqrt{2\mathrm{gy}} \tag{5.3}$$

Substituting (5.3) into (5.1) together with the identity:

$$ds = \sqrt{dx^2 + dy^2} = \sqrt{1 + y'^2}\,dx \tag{5.4}$$

This leads to the functional of the brachistochrone as follows:

$$t_{12} = \int_{P_2}^{P_1} \sqrt{\frac{1 + y'^2}{2gy}}\,dx \tag{5.5}$$

Given the rolling bead starts from rest in an xy −plane, the coordinates of the two points are then $P_1 = (0,0)$ and $P_2 = (b, B)$. The functional for the brachistochrone, along with its boundary conditions, is then expressed as:

$$T[y] = \frac{1}{\sqrt{2g}} \int_0^b \sqrt{\frac{1 + (y')^2}{y}}\,dx, \;\; y(0) = 0,\; y(b) = B \tag{5.6}$$

The function to be varied is therefore given by:

$$f = \sqrt{\frac{1 + (y')^2}{2gy}} \tag{5.7}$$

Since the function $f(y, y')$ does not depend on x, we have $\frac{\partial f}{\partial x} = 0$. Therefore, the Beltrami identity, which is a specific case of the Euler-Lagrange method, is applied to find the extremum:

$$y' \frac{\partial f}{\partial y'} - f = C \tag{5.8}$$

Then:

$$\frac{\partial f}{\partial y'} = y' \, (1 + (y')^2)^{-1/2} (2gy)^{-1/2} \tag{5.9}$$

Substituting equations (5.9) and (5.7) into (5.8) gives:

$$\frac{1}{\sqrt{2gy}\sqrt{1 + (y')^2}} = C \tag{5.10}$$

Squaring and rearranging equation (5.10) yields:

$$\left(1 + \left(\frac{dy}{dx}\right)^2\right) y = \frac{1}{2gC^2} \tag{5.11}$$

$$\left(1 + \left(\frac{dy}{dx}\right)^2\right) y = k^2 \tag{5.12}$$

The new positive constant k^2, in equation (5.12), is used to express the square of the old constant C. The following parametric equations then represent the solution to this equation:

$$x = \frac{1}{2} k^2 (2\alpha - sin\, 2\alpha) \tag{5.13}$$

$$y = \frac{1}{2}k^2(1 - cos\,2\alpha) \tag{5.14}$$

Equations (5.13) and (5.14) represent the equations of a cycloid. Additionally, it has been demonstrated in [49] that the brachistochrone problem can be extended to account for friction, resulting in the following parametric solutions:

$$x = \frac{1}{2}k^2[(\alpha - sin\,\alpha) + \mu(\alpha - cos\,\alpha)] \tag{5.15}$$

$$y = \frac{1}{2}k^2[(1 - cos\,\alpha) + \mu(\alpha + sin\,\alpha)] \tag{5.16}$$

In the context of a port crane energy management study, the frictional force is negligible when compared to the crane motor's acceleration and gravitational forces. Consequently, the optimal trajectory for port cranes is a cycloid, described by equations (5.17) and (5.18) as follows:

$$x = r(\alpha - sin\,\alpha) \tag{5.17}$$

$$y = r(1 - cos\,\alpha) \tag{5.18}$$

The constant $\frac{1}{2}k^2$ has been replaced using trigonometry with the radius r of the rolling circle that generates the cycloid curve. The optimal vertical (hoist) and horizontal (trolley) speed profiles for the crane are derived by taking the derivatives of equations (5.17) and (5.18), as shown below:

$$V_x = V_trolley = r(1 - cos\,\alpha) \tag{5.19}$$

$$V_y = V_hoist = r\,sin\,\alpha \tag{5.20}$$

The radius of the rolling circle *r* is determined based on the crane's height, the size of the ship, and the container's loading position. The parameter α represents the rotational angle of the rolling circle as the crane trolley moves horizontally between the ship and the shore. Based on the brachistochrone problem, the time required for the shipping container to travel along the cycloidal path from the ship to the shore is given by equation (5.21). In the classical brachistochrone problem, where a frictionless surface is assumed, the acceleration a equals gravitational acceleration. However, in the crane application, the resultant acceleration is derived from the crane motor's design parameters, accounting for the forces needed to hoist the shipping container. The relationship between the rotational angle α and the travel time is described by equation (5.10) [36].

$$t = 2\pi\sqrt{r/a} \tag{5.21}$$

$$\alpha(t) = t\sqrt{a/r} \tag{5.22}$$

The relationship in equation (5.22) indicates that as α increases from 0 to 2π, the optimal time required for the crane to move a shipping container between the ship and the shore depends on the radius of the rolling circle. This radius is determined by the height to which the load must be hoisted to clear the crane beams and the horizontal distance from the truck on shore to the loading position on the ship. Variations in crane height and ship-to-shore distance arise due to differences in ship sizes and port crane dimensions. Additionally, the container loading position varies because of multiple loading slots on the ship and multiple truck lanes on the shore.

The performance and energy consumption of port cranes are significantly influenced by wind, with 90 km/h being the maximum operational wind speed. Variations in container loading positions, crane height, ship dimensions, and wind speed lead to multiple optimal cycloidal load trajectories for port cranes, as shown in Figure 5.2. These multiple optimal trajectories result in corresponding variations in optimal power consumption curves. The particle swarm optimisation (PSO) technique is employed to identify the set of optimal crane trajectories and their associated energy consumption. PSO is chosen for its effectiveness in solving optimisation problems with multiple objectives and parameters.

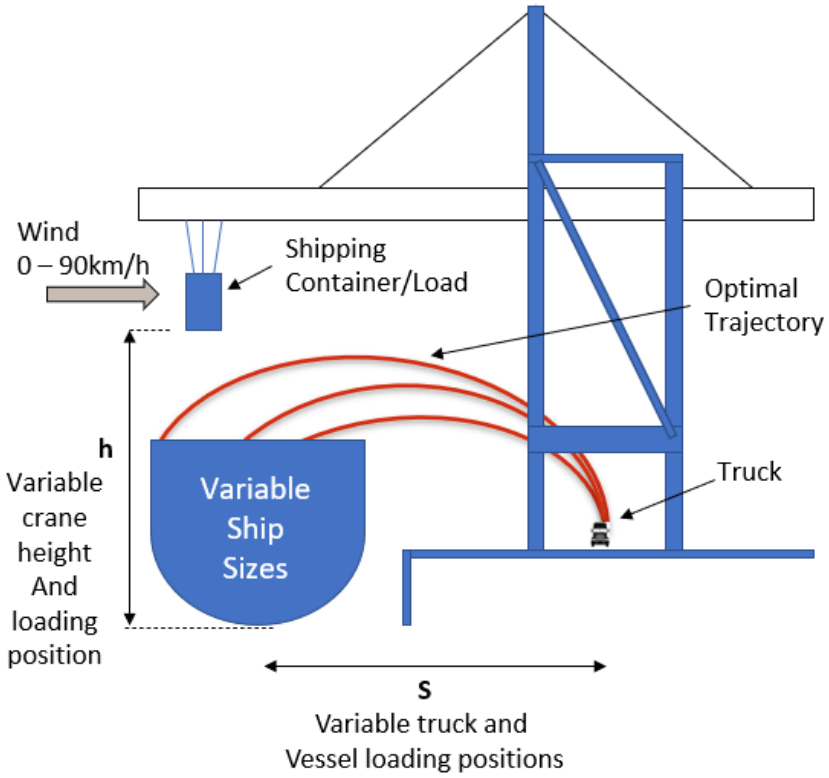


Figure 5.2: Port crane multiple optimal cycloid load trajectories

5.3 Port Crane Optimal Power Consumption

This section employs the PSO algorithm and the optimal trajectory to determine the optimal power and energy consumption for port cranes.

The PSO algorithm primarily relies on algorithm-specific hyperparameters as its inputs. User inputs include the objective function, also referred to as the fitness function. In PSO, the fitness or objective function is the criterion used to evaluate performance. This criterion is typically defined through a mathematical formula, and it quantifies system performance using a performance index [50].

For the port crane power optimisation problem, the fitness function of the PSO algorithm is formulated in equations (5.23) to (5.30). The power consumed by the port crane is described in equation (5.23), which accounts for the power used by the crane motors during hoisting and trolley operations. Equation (5.24) further expresses this power consumption in terms of the speeds and forces required for the hoisting and trolley motions.

$$P_{grid} = P_{crane_load} = P_{hoisting_motion} + P_{trolley_motion} \tag{5.23}$$

$$P_{grid} = F_{hoist}V_{hoist} + F_{trolley}V_{trolley} \tag{5.24}$$

The complete grid power consumption equation is derived by substituting equations (4.12) and (4.19) into equation (5.24) as follows:

$$P_{grid} = \frac{(M_L g + 0.5\rho c_x A(V_{hoist} + V_{wind})^2)V_{hoist}}{\eta_{ED}\eta_{GB}} + \frac{\left(M_{L+tr}(g + fg) + 0.5\rho c_x A(V_{trolley} + V_{wind})^2\right)V_{trolley}}{\eta_{ED_tr}\eta_{GB_tr}} \tag{5.25}$$

Equation (5.26), which represents the port crane's energy consumption, is utilised as the fitness function in the PSO algorithm and serves as the objective function for the optimisation problem.

$$E_{grid}(V_{trolley}, V_{hoist}, V_{wind}) = P_{grid}(V_{trolley}, V_{hoist}, V_{wind}) \times t \tag{5.26}$$

The fitness function of the PSO algorithm, as defined in equation (5.26), is subject to the following constraints:

$$0 \leq V_{hoist} \leq V_{hoist_max} \tag{5.27}$$

$$0 \leq V_{trolley} \leq V_{trolley_max} \tag{5.28}$$

$$0 \leq V_{wind} \leq V_{wind_max} \tag{5.29}$$

$$0 \leq P_{grid} \leq P_{grid_max} \tag{5.30}$$

The optimisation parameters for the PSO simulation include wind speed, the horizontal speed of the crane load, and the vertical speed of the crane load. The crane load's velocities, V_{hoist} and $V_{trolley}$, are derived from equations (5.19) and (5.20). These equations depend on two variables: the load acceleration a and the radius r, which represents the crane lifting height and the ship-to-shore distance. Practical constraints for these optimisation parameters were incorporated into the simulations. These constraints include a maximum crane lifting height of 35 m, a wind speed limit of 25 m/s, a maximum horizontal load speed of 4 m/s, and a maximum vertical load speed of 3 m/s. The PSO algorithm simulation produces a set of optimal power consumption curves. The PSO algorithm is best understood through its mathematical model, which consists of the current particle position and its velocity vector. The current particle position is determined by:

$$\overrightarrow{X_i^{t+1}} = \overrightarrow{X_i^t} + \overrightarrow{V_i^{t+1}} \tag{5.31}$$

The velocity of this particle's position is determined by:

$$\overrightarrow{V_i^{t+1}} = w\overrightarrow{V_i^t} + c_1 r_1 \left(\overrightarrow{P_i^t} - \overrightarrow{X_i^t}\right) + c_2 r_2 \left(\overrightarrow{G^t} - \overrightarrow{X_i^t}\right) \tag{5.32}$$

The pseudocode for the PSO algorithm is presented below [51]:

Algorithm 5.1: Optimal Crane Energy Consumption PSO Pseudo-Code

Initialise the optimisation problem parameters (V_{hoist}, $V_{trolley}$, V_{wind})
Initialise the limits of the optimisation parameters from equations (5.27) to (5.29)
$0 \leq V_{hoist} \leq 3\ m/s$,
$0 \leq V_{trolley} \leq 4\ m/s$
$0 \leq V_{wind} \leq 25\ m/s$
Initialise the PSO hyper-parameters (N, c1, c2, Wmin, Wmax, Vmax, and MaxIter)
Initialise the population of *N* particles
do
    for each particle
        calculate the objective or fitness of the particle using equation (5.26)
        Update PBEST if required
        Update GBEST if required
    end for
    Update the inertia weight

```
        for each particle
            Update the velocity (V)
            Update the position (X)
        end for
    while the end condition is not satisfied
    Return GBEST as the best estimation of the global optimum
```

5.4 Optimal vs. Non-Optimal Trajectory

This section compares the optimal cycloidal trajectory of the port crane with the conventional trapezoidal-shaped, non-optimal load trajectory. As previously mentioned, port productivity is measured by the number of containers a crane lifts per hour, denoted as frequency f [17]. Increasing the number of container moves per hour reduces vessel turnaround time at the port. According to [17], port cranes typically perform between 30 and 60 moves per hour. The time taken by a crane to lift and move a container between the ship and the shore is therefore expressed as:

$$T = 1/f \tag{5.33}$$

Port cranes have a dwell time of 30 seconds [17], which accounts for the time required for starting and stopping motions, locating the correct position on the truck and vessel, and ensuring clearances. The total duration, *T*, therefore, includes this 30-second dwell time in addition to the actual container movement time. In this study, the real-world crane has an average container loading duration of 33 seconds, excluding the dwell time. When the 30-second dwell time is added, the total loading duration becomes 63 seconds.

Table 5.1: Optimal Trajectory Load Cycle Duration

Ship to shore distance (m)	**Minimum**	**Average**	**Maximum**
	20	50	100
Cycloid radius i.e half crane lifting height (m)	3.2	8.0	15.9
Actual crane moving time (s)	9.8	15.5	21.9
Dwell time (s)	30	30	30
Total duration of crane move (s)	39.8	45.5	51.9

Figure 5.3 presents the average moves per hour achieved by port cranes globally [52]. The highest average performance recorded was 24.2 moves per hour for ships carrying between 8 501 and 135 000 shipping containers. Using equation (5.33), the optimal trajectory load cycle duration is calculated and summarised in Table 5.1. The real-world crane dimensions are utilised to determine the minimum, average, and maximum container loading distances between the ship and the truck on shore, which are 20 m, 50 m, and 100 m, respectively.

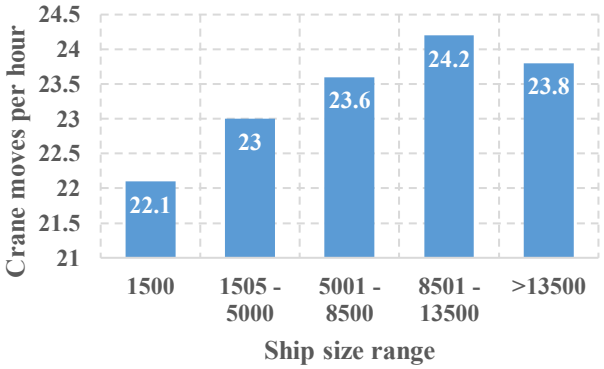
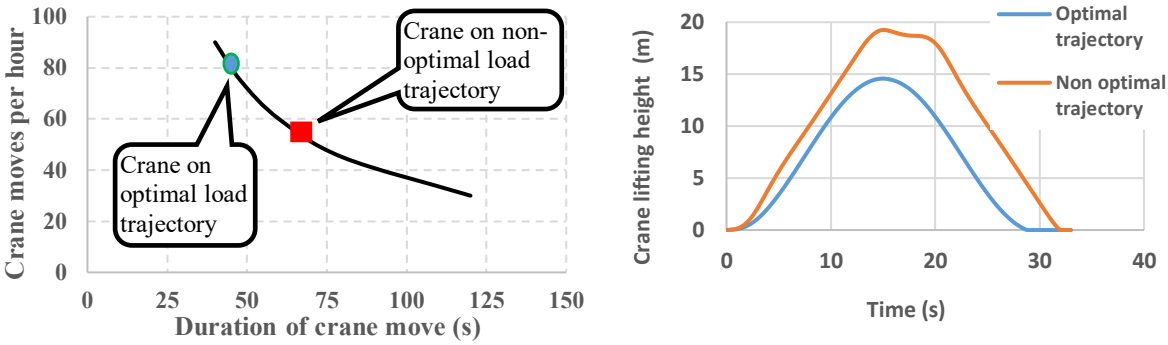


Figure 5.3: Real-world crane loading frequency per ship size [52]

The hoisting gear lifting height of the real-world crane is used to calculate the radius of the optimal cycloidal trajectory. The results indicate that a crane following the optimal load trajectory would have a load cycle duration ranging between 39.8 seconds and 51.9 seconds. Figure 5.4a compares the optimal and non-optimal crane load trajectories along the crane productivity curve, which was developed using typical crane performance data from [17]. Based on load cycle durations of 63 seconds for the non-optimal trajectory and 45.5 seconds for the optimal trajectory, the corresponding crane productivity rates are 57 moves per hour and 79 moves per hour, respectively, as calculated using equation (5.33).



(a) (b)

Figure 5.4: Optimal vs. non-optimal crane trajectories, (a) crane productivity curve-based comparison (b) trajectory-based comparison

This represents a 38.59% improvement in speed and productivity for the optimal crane load trajectory. Figure 5.4b illustrates that, compared to the non-optimal trajectory, the optimal trajectory features a smoother shape, requires less time, and involves a lower lifting height to complete a crane move.

5.5 Simulation Results

This section presents the MATLAB simulation results. The particle swarm optimisation (PSO) algorithm was applied to identify the set of Pareto-optimal crane trajectories, accounting for variations in crane size, ship size, and wind speed. The crane's optimal grid power consumption, described by equation (5.25), served as the objective function in the PSO simulation. The results include a set of Pareto-optimal crane trajectories, illustrated in Figure 5.5a, where each of the 500 dots represents an optimal cycloidal trajectory as shown in Figure 5.2. Figure 5.5b displays the corresponding optimal energy consumption for each of the 500 Pareto-optimal trajectories.

The Pareto-optimal solutions in Figure 5.5a provide a general guideline for crane designers. These guidelines allow designers to select a crane based on its energy consumption and determine its corresponding size and maximum wind speed limit. Conversely, designers can input crane size and wind speed parameters to obtain the crane's optimal energy consumption. The wind boundary condition in Figure 5.5a is based on port cranes not operating beyond 90 km/h wind speeds (gale force).

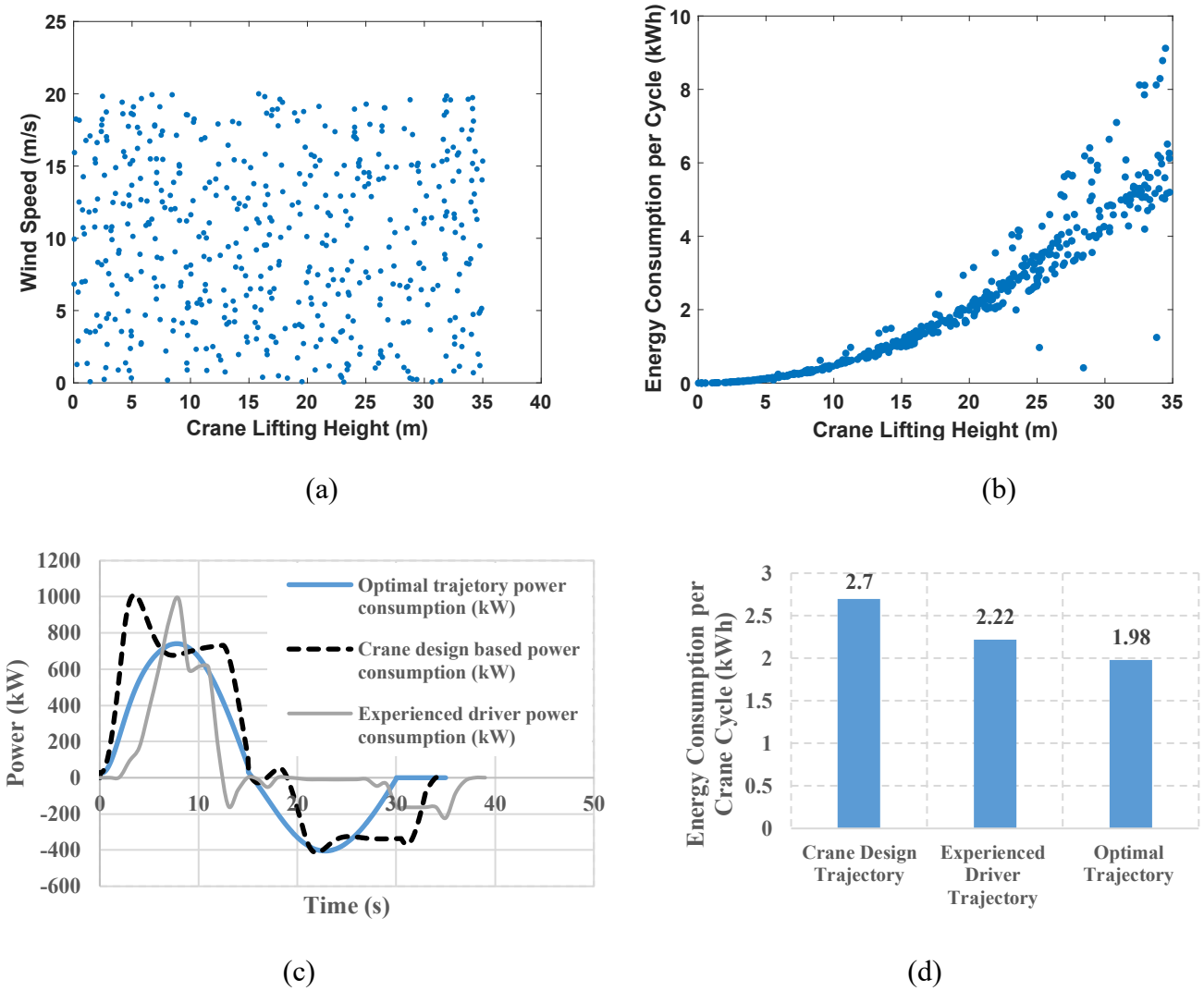


Figure 5.5: Simulation results, (a) A set of pareto optimal solutions (b) Optimal power consumption trajectories (c) Comparing optimal and non-optimal crane trajectories power consumption (d) Comparing optimal and non-optimal crane trajectories energy consumption

The maximum lifting height of 35 m corresponds to current maximum container ship sizes, though this parameter can be adjusted by designers. The mean energy consumption for the optimal trajectory is 2.25 kWh, with a maximum of 9.17 kWh. The MATLAB Simulink EMR library was used to simulate the port crane's EMR-based model shown in Figure 4.2. This simulation compared a real-world crane with a crane following the optimal trajectory obtained using the real-world crane parameters in the PSO simulation. Figure 5.5c and Figure 5.5d present the simulation results.

The optimal trajectory reduces the crane's peak power consumption by 36.38% compared to the non-optimal trajectory. As shown in Figure 5.5d, a crane on the optimal trajectory consumes

1.98 kWh per load cycle, which represents a 26.67% reduction compared to the 2.70 kWh consumed by cranes using a non-optimal trajectory. Additionally, the optimal trajectory uses 10.81% less energy than an experienced crane driver. The optimal trajectory also achieves a faster load handling time of 30 seconds compared to 35 seconds and 40 seconds for the non-optimal simulated trajectories. Furthermore, the smooth sinusoidal power consumption curve of the optimal trajectory underscores the need for crane automation to reduce dynamic power fluctuations caused by non-optimal trajectories and human drivers.

5.6 Chapter Summary

This chapter focused on developing the optimal load trajectory for port cranes, which was identified as a cycloidal path. The key findings from this chapter are as follows:

- The developed optimal crane load trajectory is 38.59% faster and more productive compared to the non-optimal trajectory.
- The optimal trajectory reduces the crane's peak power consumption by 36.38% relative to the non-optimal trajectory.
- The optimal trajectory reduces the crane's energy consumption by 26.67% compared to the non-optimal trajectory and by 10.81% compared to trajectories followed by experienced crane drivers.
- The sinusoidal speed reference curves derived from the cycloid trajectory can serve as a guide for automating port crane systems.
- The outcomes of this study provide guidelines for port crane designers, enabling the selection of cranes based on energy consumption requirements, maximum wind speed tolerance, crane lifting height, and the trolley distance between the ship and the shore.

6. Energy Consumption Optimization Strategy for Port Cranes Based on Pontryagin's Minimum Principle and Filtering Strategies

This chapter develops an energy management strategy for port cranes. The objective is to optimise the crane's energy consumption and reduce its energy consumption from the grid. The objective is achieved by applying a battery-supercapacitor hybrid energy storage system (H-ESS) and a combination of filtering and Pontryagin's Minimum Principle (PMP) energy management strategies (EMSs) to the port crane. The filtering-based EMS manages the power split between the grid and the H-ESS, while the PMP-based EMS manages the power split between the battery and supercapacitor inside the H-ESS. Overall, the proposed EMS has a simple analytical cost function, is computationally fast, and is easier to implement while producing optimal and effective results.

6.1 Port Crane System EMR-based Model

This chapter extends the EMR-based port crane model developed in Chapter 4 by adding to it the battery-supercapacitor H-ESS. The parameters of the H-ESS are shown in Table 6.1 and are obtained from real-world battery and supercapacitor systems used in similar previous studies [12]. All other port crane subsystems are described and modelled in Chapter 4. Figure 6.1 illustrates the port crane model based on EMR after adding the H-ESS. This model yields the system's mathematical representation, separating the EMS and local control layers. The EMS operates at the supervisory level or a higher layer than the local control system, with each layer possessing distinct dynamics that require unique treatment.

Table 6.1: H-ESS parameters

Batteries - Lithium iron phosphate (LiFePO4) battery	
Battery bank capacity	1 600 Ah
Battery bank rated energy	935.36 kWh
Battery bank rated voltage	584.6 V
Supercapacitors	
SC rated energy	7.09 kWh
SC rated voltage	756 V

SC rated capacity	89.29 Ah

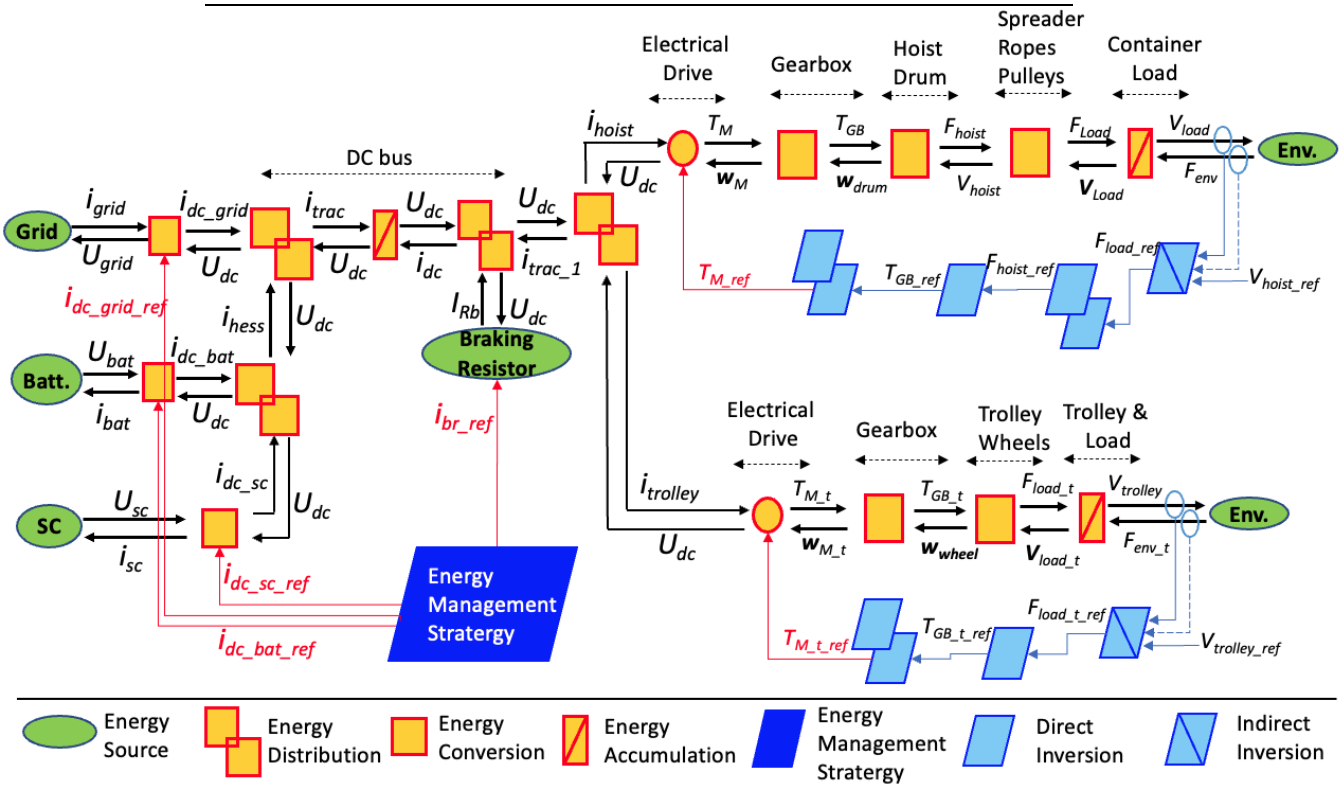


Figure 6.1: EMR model of the port crane and its inversion-based local control system

6.2 H-ESS Mathematical Modelling

Chapter 3 shows the mathematical models for all other port crane systems. This section presents the mathematical models for the additional battery-supercapacitor H-ESS. The mathematical equations used to model the port crane's H-ESS are shown in Table 6.2. The battery pack is modelled by equation (6.1**)**, where the output is the voltage U_{bat} and its input is the current $\mathrm{i_{bat}}$. The battery's internal voltage drop occurs across r_{bat} which is the equivalent series resistance (ESR). Both ESR and open-circuit voltage (OCV), represented by $U_{OC_{bat}}$ are non-linear functions of the battery's state of charge (SoC). Look-up tables are used to obtain the relationships $U_{OC_{bat}}SoC_{bat}$ and $r_{bat}SoC_{bat}$. The battery SoC in equation (6.2**)** is calculated using the coulomb counting method.

The supercapacitor pack is modelled by equation (6.3**)**. The SoC and voltage of the SC are proportional. The current i_{SC} charges and discharges the SC with capacitance C_{SC} and output

voltage U_{SC}. The internal resistance r_{SC} of the SC is obtained from the manufacturer's datasheets. It causes a voltage drop, but does not depend on the supercapacitor SoC. The choppers for the SC and battery are modelled by equations (6.4**)** and (6.5**)**, respectively. These choppers are perfectly controlled and modelled using static models with immediate response to current references provided by the EMS. The dc-bus is modelled by equation (6.6**),** showing that the hoist motor current is given by the current from the three energy sources, less the current consumed by the braking resistor and the DC-bus capacitor. The voltage on the DC-bus U_{dc} is common. The port crane system disturbances and local control systems are shown in Chapter 3.

Table 6.2: H-ESS mathematical modelling equations

Battery	$U_{bat} = U_{OC_{bat}} SoC_{bat} - r_{bat} SoC_{bat} i_{bat}$	(6.1)
	$SoC_{bat} = SoC_{bat\ init} - \frac{100}{3600 C_{bat}} \int i_{bat}\, dt$	(6.2)
SCs	$U_{SC} = U_{SC\ init} - \frac{1}{C_{SC}} \int i_{SC}\, dt - r_{SC} i_{SC}$	(6.3)
Chopper	$i_{dc_X} = i_{X_{ref}}\ with\ X \in [bat, SC]$	(6.4)
	$i_X = \frac{U_{dc} i_{dc_X}}{\eta_{dc_X}^k U_X} \begin{cases} k = 1 & U_{dc} i_{dc_X} \geq 0 \\ k = -1 & U_{dc} i_{dc_X} < 0 \end{cases}$	(6.5)
DC bus	$i_{trac_1} = i_{grid} + i_{HESS} - C_{dc} \frac{d}{dt} U_{dc} - i_{Rb}$	(6.6)

6.3 Proposed PMP-based Energy Management Strategy

The next two sections develop an energy management strategy for a port crane with an electrical powertrain connected to a grid supply and an H-ESS consisting of batteries and supercapacitors, as shown in Figure 6.2. The energy distribution between the battery and supercapacitor, as illustrated in Figure 6.3 is managed by a PMP strategy. The braking strategy directs excess regenerative energy in the DC-bus that the H-ESS does not consume, to the braking resistor. The H-ESS is primarily charged using the crane's regenerative braking energy. The objective of this study is to minimise grid power P_{grid}, which is given by equation (6.7). This is achieved using the battery and supercapacitor in the H-ESS, as shown in equations (6.7) and (6.8). Without the H-ESS, the crane's grid power consumption is equal to its traction power.

$$P_{grid} = P_{trac} - P_{HESS} \tag{6.7}$$

$$P_{HESS} = P_{bat} + P_{sc} \tag{6.8}$$

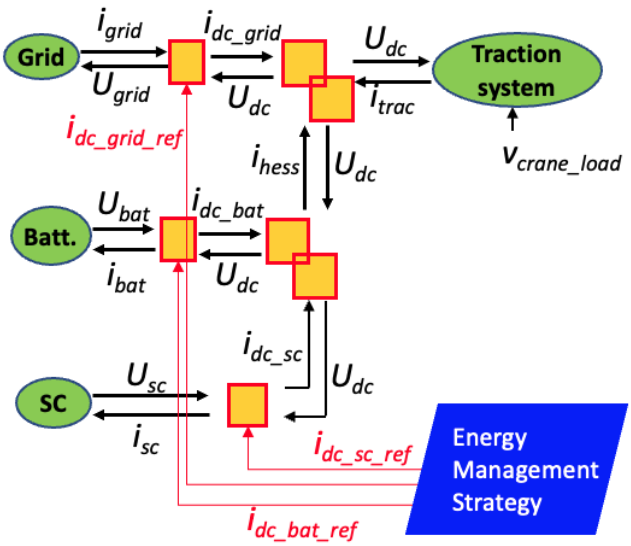


Figure 6.2: Reduced port crane EMR model used for EMS development

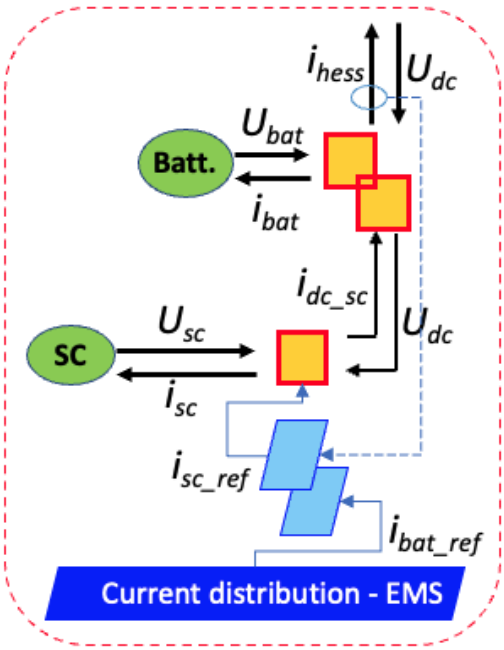


Figure 6.3: Port crane EMR model used for PMP strategy development

The DC-bus voltage U_{dc} is kept constant for system stability. Therefore, the objective of this study is to minimise of grid current i_{grid}. This is achieved by maximizing the H-ESS current i_{HESS} as shown in equation (6.9). However, within the H-ESS, the characteristics of the battery and supercapacitor must be carefully considered. These characteristics include their energy densities, power densities, cycling times, and battery life, as can be observed in a Ragone plot [53].

Port cranes have a power demand profile with a peak of about 2 MW and load cycle time well below 60 s [2]. The result of considering the ESS characteristics against the crane power demand profile is that the supercapacitor in the H-ESS is used to support the battery life, which means that i_{sc} in equation (6.10) is maximized, while i_{bat} needs to be minimized. In summary, the objective of this study is to minimize the crane's grid power consumption, with the sub-objective of maximizing battery life.

$$i_{grid} = i_{trac} - i_{HESS} \tag{6.9}$$

$$i_{HESS} = i_{bat} + i_{sc} \tag{6.10}$$

First, this chapter uses the PMP approach to develop an EMS for current distribution between the battery i_{bat} and supercapacitor i_{sc} within the H-ESS, as shown in equation (6.10). The next chapter uses the filtering strategy to determine the current distribution between the grid i_{grid} and H-ESS i_{HESS} as shown in equation (6.9). The EMS model was selected to achieve optimal results using EMSs that are computationally fast and easier to implement.

6.3.1 Problem Formulation

6.3.1.1 Mathematical System Dynamics

To apply optimal control theory effectively, it is essential to formulate the energy management issue as an optimal control problem. This involves representing the system's dynamic model as a set of equality constraints, while the boundaries on state and control variables act as inequality constraints. In this research, these constraints are managed using the traditional approach detailed in [54]. Consequently, only the equality constraint, which represents the system's

dynamic model, needs to be specified. Utilizing the simplified illustration in Figure 6.3**,** based on equations (6.3) and (6.5), and assuming that the series resistance r_{sc} of the SCs is negligible, and the SCs start in a discharged state, the reduced mathematical model of the system can be deduced as shown in equation (6.11):

$$\frac{d}{dt}u_{sc} = -u_{bat}\frac{\eta_{conv}^{k}}{C_{sc}}\frac{i_{sc\,ref}}{u_{sc}} \tag{6.11}$$

where u_{sc} is the state variable, $i_{sc\,ref}$ is the control variable, and u_{bat} is the disturbance input. The effect of resistance is not considered.

6.3.1.2 Cost Function – Performance Criterion

Since the objective of adding the supercapacitor to the H-ESS is to extend battery life, the root mean square (RMS) value of the battery current serves as the applicable performance criterion:

$$I_{bat\,rms} = \sqrt{\frac{1}{t_f - t_0}\int_{t_0}^{t_f} i_{bat}^2 dt} \tag{6.12}$$

where t_0 and t_f denote the initial and final times, respectively. Additionally, quadratic functions hold significance in many optimisation strategies [55]. Therefore, the cost function for the studied energy management problem of the port crane is formulated as follows:

$$J = \int_{t_0}^{t_f} i_{bat}^2 dt \tag{6.13}$$

The PMP-based EMS in this study formulates the optimal control problem of energy management for the H-ESS by determining the optimal control law for the battery/supercapacitor H-ESS using the dynamic model shown in equation (6.12) to minimise the cost function given in equation (6.13).

6.3.2 EMS Development Using PMP

6.3.2.1 Methodology

First, a concise overview of the general background concerning Pontryagin's Minimum Principle (PMP) is provided. This pertains to a dynamical system:

$$\frac{d}{dt}x = f(x, w, t) \tag{6.14}$$

where *x* represents the state variable and w denotes the control variable, with the cost function defined as:

$$J = h\left(x\left(t_f\right), t_f\right) + \int_{t0}^{tf} g(x, w, t)dt \tag{6.15}$$

where the function h represents the cost associated with the final state $x\left(t_f\right)$, and the function g denotes the integral cost of progression. Subsequently, a Hamiltonian function is established as follows:

$$H = g(x, w, t) + \lambda f(x, w, t) \tag{6.16}$$

where λ represents the co-state variable. According to PMP, if an optimal control law $w*$ exists, it must adhere to the following three conditions:

$$\frac{d}{dt}x^* = \frac{\partial H(x^*, w^*, \lambda^*, t)}{\partial \lambda} \tag{6.17}$$

$$\frac{d}{dt}\lambda^* = \frac{\partial H(x^*, w^*, \lambda^*, t)}{\partial x} \tag{6.18}$$

$$H(x^*, w^*, \lambda^*, t) \leq H(x^*, w, \lambda^*, t) \tag{6.19}$$

6.3.2.2 EMS Development

Taking into account the system model (6.11) and the cost function (6.12), the Hamiltonian is expressed with the co-state variable λ as follows:

$$H = i_{bat}^2 - \lambda \frac{u_{bat}}{C_{sc}} \frac{i_{sc\,ref}}{u_{sc}} \tag{6.20}$$

The necessary condition (6.19) of the Hamiltonian minimisation is realised by:

$$\frac{\partial H}{\partial i_{sc\,ref}} = 0 \tag{6.21}$$

The left-hand side of equation (6.21)is derived from:

$$i_{bat} = i_{hess} - i_{dc_{sc}} \tag{6.22}$$

Given that i_{hess} is the disturbance that does not depend on the control variable $i_{sc\,ref}$ and assuming a perfectly controlled supercapacitor chopper with a perfect response and without delay, that leads to:

$$\frac{\partial (i_{bat}^2)}{\partial i_{sc\,ref}} = -2 i_{bat} \tag{6.23}$$

The partial derivative to be calculated therefore becomes:

$$\frac{\partial H}{\partial i_{sc\,ref}} = -2 i_{bat} - \lambda \frac{u_{bat}}{C_{sc}} \frac{i_{sc\,ref} \frac{\partial u_{sc}}{\partial i_{sc\,ref}} - u_{sc}}{u_{sc}^2} \tag{6.24}$$

The partial derivative of u_{sc} with respect to $i_{sc\,ref}$ is computed by:

$$\frac{\partial u_{sc}}{\partial i_{sc\,ref}} = \frac{1}{\frac{\partial \frac{u_{sc}}{u_{bat}} i_{sc}}{\partial u_{sc}}} = \frac{1}{\frac{i_{sc}}{u_{bat}} + \frac{u_{sc}}{u_{bat}} \frac{\partial i_{sc}}{\partial u_{sc}}} \tag{6.25}$$

The partial derivative of i_{sc} with respect to u_{sc} was derived in [54] and is expressed as follows:

$$\frac{\partial i_{sc}}{\partial u_{sc}} = -\frac{i_{sc}}{\sqrt{u_{sc}^2 - 4r_{sc}P_{sc}}} \tag{6.26}$$

Applying equation (6.26) to equation (6.25) leads to:

$$\frac{\partial u_{sc}}{\partial i_{sc\,ref}} = \frac{u_{bat}\sqrt{u_{sc}^2 - 4r_{sc}P_{sc}}}{i_{sc}\sqrt{u_{sc}^2 - 4r_{sc}P_{sc} - P_{sc}}} \tag{6.27}$$

The partial derivative of the Hamiltonian then becomes:

$$\frac{\partial H}{\partial i_{sc\,ref}} = -2i_{bat} - \lambda \frac{u_{bat}}{C_{sc}} \frac{i_{sc\,ref} \frac{u_{bat}\sqrt{u_{sc}^2 - 4r_{sc}P_{sc}}}{i_{sc}\sqrt{u_{sc}^2 - 4r_{sc}P_{sc} - P_{sc}}} - u_{sc}}{u_{sc}^2} \tag{6.28}$$

Given the control setup illustrated in Figure 6.3, the EMS determines the current reference for the batteries, denoted as $i_{bat\,ref}$. Subsequently, $i_{sc\,ref}$ is acquired by compensating for the measured traction current as follows:

$$i_{sc_{ref}} = i_{hess_{meas}} - i_{bat_{ref}} \tag{6.29}$$

Thus, the control law should be:

$$i_{bat_{ref}} = -\lambda \frac{u_{bat}}{2C_{sc}} \frac{\frac{i_{dc_{sc}} u_{bat}\sqrt{u_{sc}^2 - 4r_{sc}u_{sc}i_{sc}}}{i_{sc}\sqrt{u_{sc}^2 - 4r_{sc}u_{sc}i_{sc} - u_{sc}i_{sc}}} - u_{sc}}{u_{sc}^2} \tag{6.30}$$

However:

$$\frac{i_{dc\,sc}}{i_{sc}} = \frac{u_{sc}}{u_{bat}} \tag{6.31}$$

Assuming ideal conversion, the control law (6.30) is then defined by:

$$i_{bat_{ref}} = \lambda \frac{u_{bat}}{2C_{sc}} \frac{u_{sc} - \frac{u_{sc}\sqrt{u_{sc}^2 - 4r_{sc}u_{sc}i_{sc}}}{\sqrt{u_{sc}^2 - 4r_{sc}u_{sc}i_{sc}} - u_{sc}i_{sc}}}{u_{sc}^2} \tag{6.32}$$

The co-state variable λ is required to complete the control law in equation (6.32). Previous studies in [12] and [54] have shown that λ is determined as:

$$\lambda = C_{sc} i_{hess_{rms}} \tag{6.33}$$

where, $i_{hess_{rms}}$ is contingent upon the driving modes and is determined in advance through the utilisation of the standard crane cycle.

6.3.3 PMP EMS Implementation

The energy management strategy based on PMP described above is presented in an analytical format, involving straightforward mathematical computations. This simplicity facilitates its integration, as illustrated in Figure 6.4, where it fits into the current distribution strategy block depicted in Figure 6.3. Three sensors are required for the measurement of the supercapacitor voltage (u_{sc}), battery voltage (u_{bat}), and supercapacitor current (i_{sc}), enabling the computation of the control variable $i_{bat\ ref\ calc}$ using equations (6.28) and (6.29). An additional sensor for $i_{\text{hess meas}}$ is only engaged when the supercapacitor voltage reaches its limits. Under such circumstances, $i_{bat\ ref}$ transitions from $i_{bat\ ref\ calc}$ to the measured value of $i_{hess_{meas}}$.

6.4 Proposed Filtering-based Grid/H-ESS Energy Management Strategy

The filtering-based EMS was selected for this study because it is among the most classical deterministic rule-based EMSs [56], [57]. It is not complex and can be easily implemented whilst delivering effective near-optimal results [56], [57]. The filter smooths out the output of the H-ESS, reducing stress on the H-ESS components [58]. Additionally, the filter reduces the noise and disturbances in the H-ESS output, which can otherwise lead to inefficient operation [58]. It serves as an effective control strategy that enhances the performance of the H-ESS by decreasing peak power demands, boosting efficiency, and improving reliability [58].

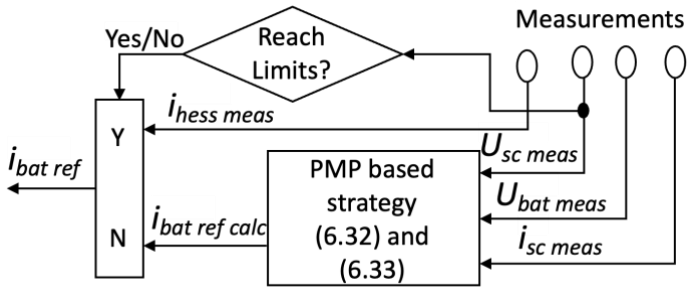


Figure 6.4: PMP-based EMS for power split management in the batt-SC H-ESS

6.4.1 H-ESS Model Reduction

To develop the strategy for the power split between the H-ESS and the grid, the H-ESS is first reduced to an equivalent ESS. As depicted in Figure 6.5, the H-ESS model is simplified to an equivalent ESS, where the capacitance $C_{ESS\,eq}$ is expressed in Farads. Since the capacitance of the supercapacitors (in Farads) is notably smaller than that of the batteries (in kilo-Farads), the equivalent ESS capacitance $C_{ESS\,eq}$ can be regarded as equivalent to that of the batteries, given by:

$$C_{ESS_{eq}} = C_{bat_{eq}} = 3600 C_{bat} \tag{6.34}$$

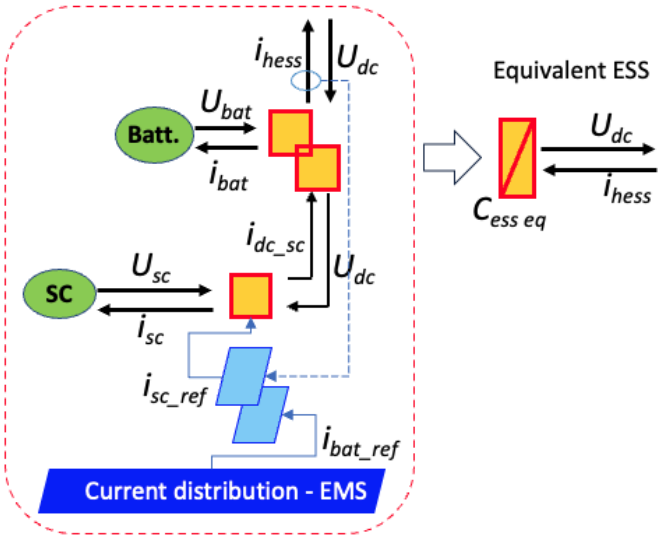


Figure 6.5: H-ESS reduction to an equivalent ESS given the battery's dominant capacitance

6.4.2 Filtering EMS development

Reducing the H-ESS to an equivalent capacitance $C_{ESS\,eq}$ results in the reduced port crane model shown in Figure 6.5**.** The filtering strategy is developed based on the fact that energy storage devices have different frequency characteristics [59].

This can be achieved through the implementation of a low-pass filter (LPF) as follows:

$$i_{hess_{ref}} = \frac{1}{\tau_{LPF}s + 1} i_{trac_{meas}} \tag{6.35}$$

where τ_{LPF} is the LPF time constant given by:

$$\tau_{LPF} = {}^{1}/_{2\pi f_{LPF}} \tag{6.36}$$

The LPF cut-off frequency f_{LPF} can be determined using the Ragone plot [60], iterative examinations [43], or adaptive studies [61]. Figure 6.6 shows a Ragone plot depicting various energy storage systems. The Ragone plot illustrates that batteries have high energy density but low power density, whereas supercapacitors exhibit characteristics of low energy density but high-power density. Using the Ragone plot, the cut-off frequency is determined as follows:

$$f_{LPF} = \frac{\rho_{power}\left[\frac{W}{kg}\right]}{\rho_{energy}\left[\frac{J}{kg}\right]} \tag{6.37}$$

where f_{LPF} represents the cut-off frequency derived from the Ragone plot, and ρ_{power} and ρ_{energy} denote the power density and energy density, respectively [53]. Considering previous studies [43] with similar drivetrains, the cut-off frequency of $f_{LPF} = 48\ miliHz$ is used in this study. The LPF time constant is given by equation (6.36) and it is therefore 3.316 s.

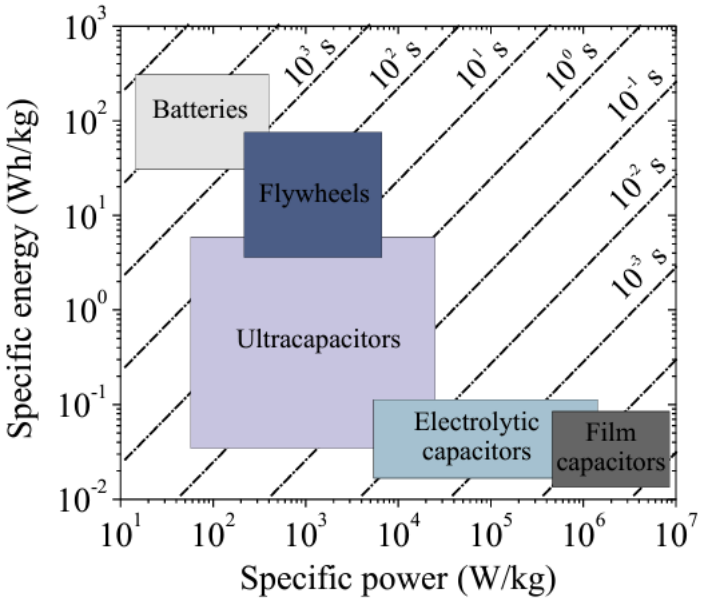


Figure 6.6: Ragone Plot showing the ESS power and energy densities [53]

6.4.3 Braking Strategy

The aim of the braking strategy is to maximise energy regeneration. During crane's regenerative mode, where i_{grid} equals zero, the excess regenerative energy that is not absorbed by the H-ESS is burnt in the braking resistor as shown in equation (6.38).

$$i_{Rb} = i_{trac} - i_{hess} \tag{6.38}$$

6.4.4 Filtering And Braking Strategies Implementation

Figure 6.7 shows the resultant reduced crane EMR used for the filtering strategy implementation. Figure 6.8, shows the details of the filtering strategy block in Figure 6.7. Equation (6.38) is calculated in the EMS block in Figure 6.1. and the braking resistor current is supplied to the breaking resistor block with i_{Rb} being equal to $i_{rb_{ref}}$. The resultant i_{hess} from the filtering strategy is used in the PMP strategy in the previous chapter to determine the power split between the battery and supercapacitor.

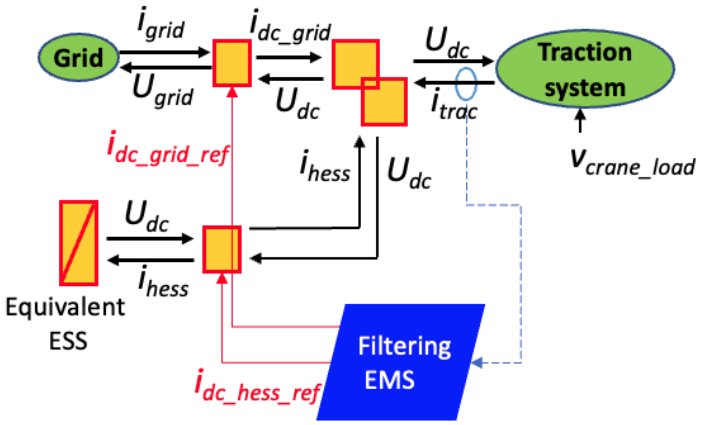


Figure 6.7: Reduced port crane EMR model showing the filtering strategy development implementation

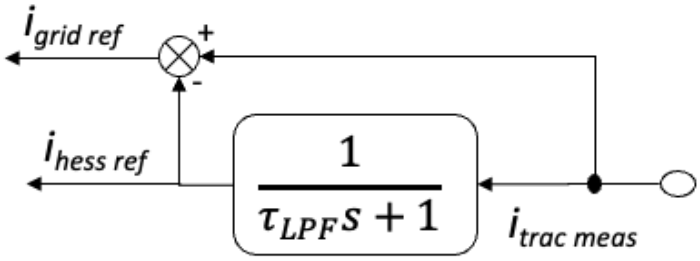


Figure 6.8: Implementation of the filtering strategy to manage the power split between the grid and the H-ESS

Figure 6.9 summarises the implementation of the combined filtering and PMP energy management strategy for port cranes. The two steps to implementing the EMS for port cranes are as shown in Figure 6.9. First the current distribution between the grid and the H-ESS is

determined using the filtering strategy, then the current distribution between the battery and the supercapacitor is determined using the PMP strategy. Furthermore, the EMS enhances the performance of the H-ESS by decreasing peak power demands, boosting efficiency, improving reliability, and extending its lifespan, making H-ESS more dependable and cost-efficient.

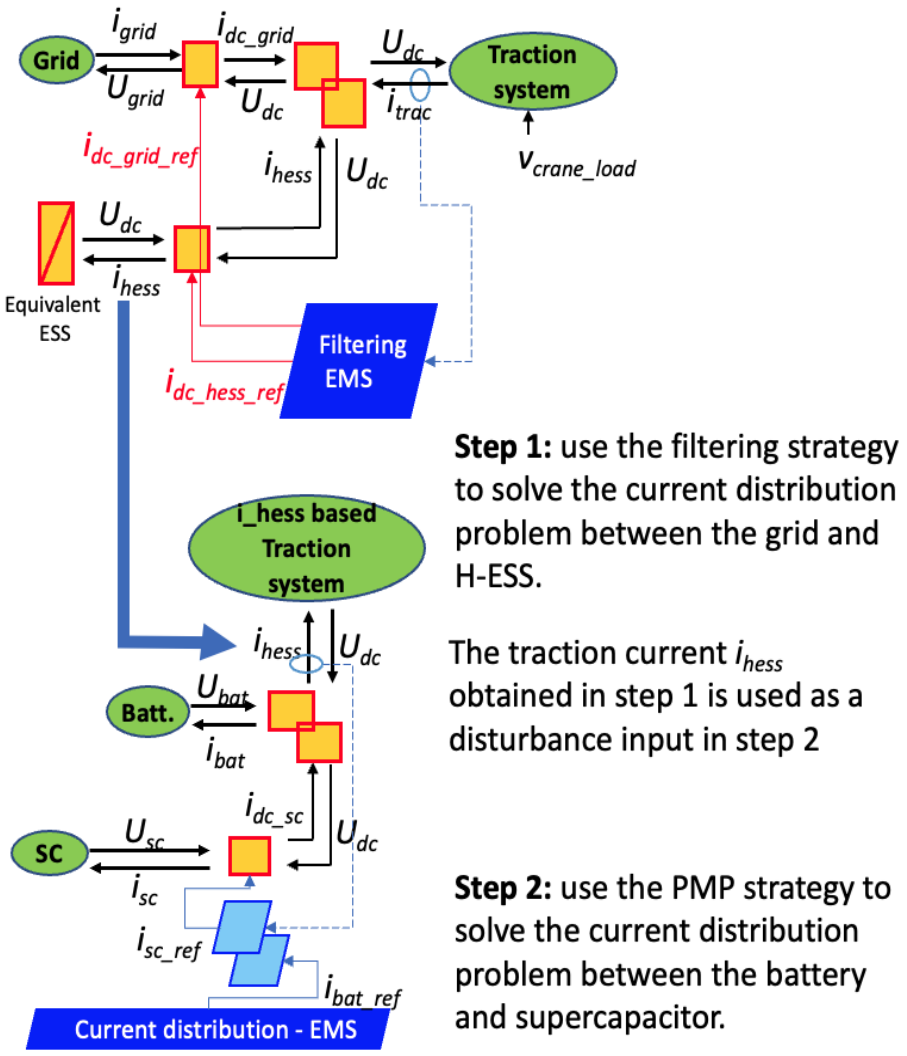


Figure 6.9: Step-by-step implementation of the combined EMS comprising of the filtering and the PMP-based sub-EMSs

6.5 EMS Strategy Implementation

Given the validated EMR model and the two energy management strategies developed in the sections above, this section uses the EMR-based crane model to implement the combined energy consumption optimisation strategy. The EMR port crane model shown in Figure 6.1. was used for Matlab Simulink simulations. The energy management strategies were applied in the Matlab simulations as described above. Figure 6.10. shows that by including an H-ESS with the EMS developed above in the port crane power train, the port crane's energy consumption from the utility grid has decreased by 29%.

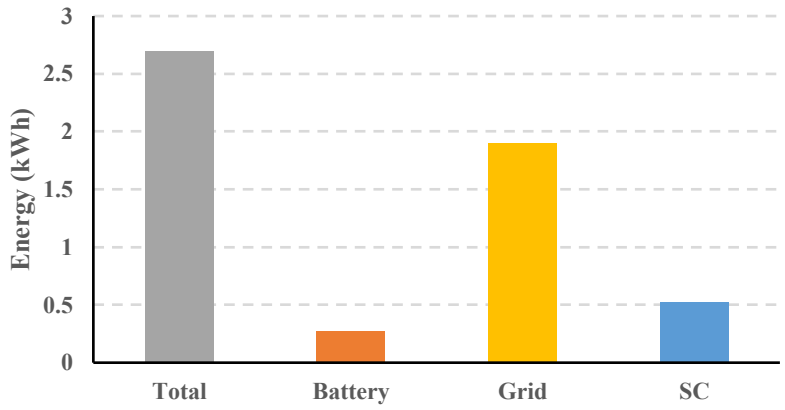


Figure 6.10: Port crane energy consumption for one load cycle

Figure 6.11 shows that the crane's peak power consumption from the utility grid has decreased by 29.6%. Figure 6.12 shows the battery and supercapacitor states of charge. The supercapacitor gets discharged and recharged by 26%, while the battery gets discharged and recharged by 8%. The battery and supercapacitor SoC results confirm that the EMS is preserving battery life by maximising the supercapacitor utilisation. The recharging of the battery and supercapacitor, which occurs from 18 s onwards, confirms the capturing of the cranes' regenerative energy by the H-ESS. Lastly, since STS cranes are the largest port cranes with about 2 MW power demand and use a common drivetrain found in many types of port and industry cranes, the EMS developed in this study is applicable to other types of cranes.

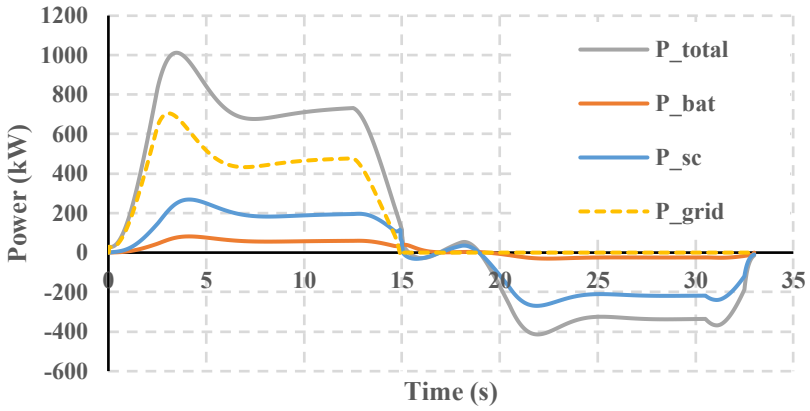


Figure 6.11: Port crane simulated power consumption

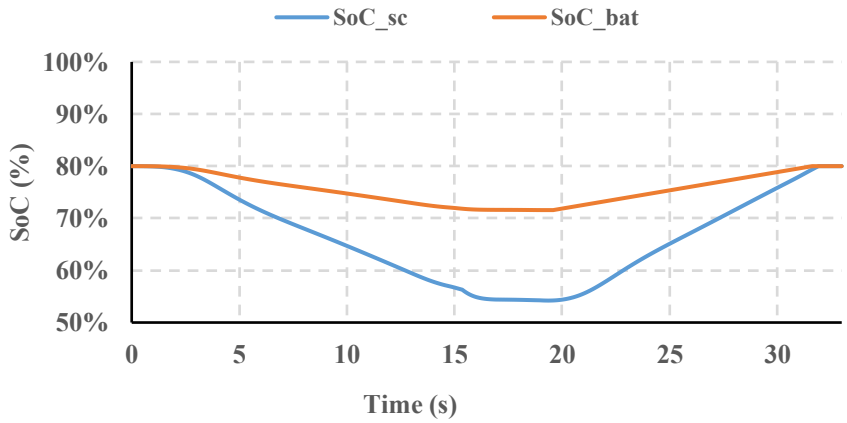


Figure 6.12: One load cycle battery and supercapacitor SOCs

6.6 Chapter Summary

This chapter presents an energy management strategy for port cranes, with the objective of managing the energy distribution between the grid and an H-ESS comprised of both a battery and a supercapacitor. The sub-objective of the EMS is to extend battery life. The developed energy management strategy combines filtering and Pontryagin Minimum Principle strategies. The results of applying the EMS and H-ESS to the port crane powertrain are as follows:

- The port crane's energy consumption from the utility grid decreased by 29%.
- The peak power consumption from the utility grid decreased by 29.6%.

- During the crane load handling cycle, the supercapacitor and the battery were discharged and recharged by 26% and 8%, respectively. The recharge was due to regenerative braking energy.
- Given that STS cranes are the largest port cranes, with about 2 MW power demand and share a common drivetrain with many types of port and industry cranes, the EMS developed in this study is applicable to other types of cranes.

Overall, the proposed EMS model for this study has a simple analytical cost function, is computationally fast, and is easier to implement while producing optimal and effective results. Furthermore, the EMS enhances the performance of the H-ESS by boosting efficiency, improving reliability, and extending its lifespan, making H-ESS more dependable and cost-efficient.

7. Optimal Sizing of the Port Crane's Battery/Supercapacitor H-ESS

The previous chapters developed an in-depth model of the port crane system, including the H-ESS comprising the battery and supercapacitor and the associated EMSs as shown in Figure 7.1. This chapter focuses on developing a generalised optimal sizing technique for these two energy storage devices.

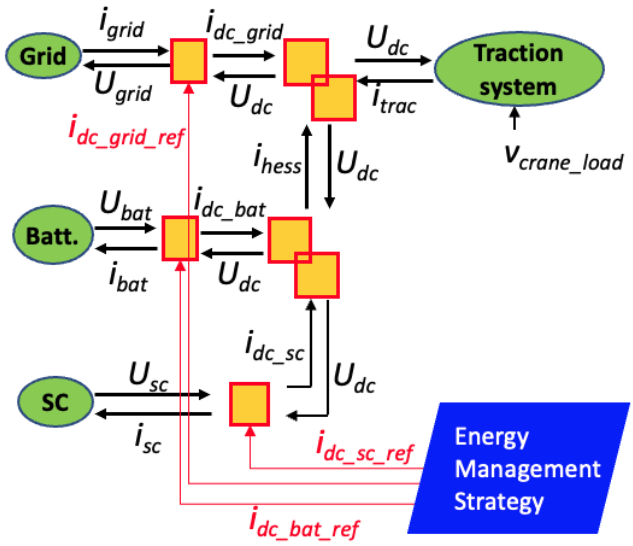


Figure 7.1: Reduced port crane EMR model

7.1 Battery and Supercapacitor Models

Figure 7.2 shows the equivalent circuit of the supercapacitor pack, which consists of series-connected modules (n_{SC_s}) and parallel-connected branches (n_{SC_p}).

The supercapacitor electrical model is described by:

$$U_{module} = U_{module_0} - i_{module} r_{esr} - \frac{1}{C_{rated}} \int i_{module}\, dt \tag{7.1}$$

$$U_{sc} = U_{module} n_{sc_s} \tag{7.2}$$

$$i_{module} = i_{sc} / n_{sc_p} \tag{7.3}$$

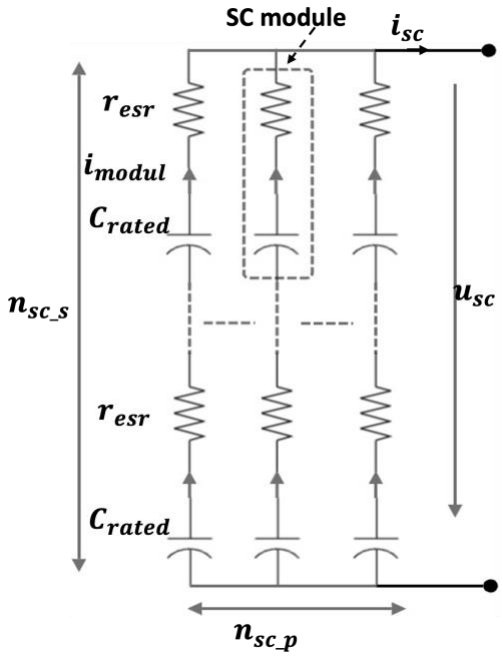


Figure 7.2: Supercapacitor pack equivalent circuit [62]

Similarly, Figure 7.3 shows the equivalent circuit of the battery pack, which consists of series-connected modules (n_{bat_s}) and parallel-connected branches (n_{bat_p}).

The battery electrical model is described by:

$$U_{cell} = U_{OCV}(SoC) - i_{cell} r_{cell} \tag{7.4}$$

$$SoC = SoC_0 - \frac{100\%}{3600\, Q_{rated}} \int i_{cell}\, dt \tag{7.5}$$

$$U_{bat} = U_{cell} n_{bat_s} \tag{7.6}$$

$$i_{cell} = i_{bat} / n_{bat_p} \tag{7.7}$$

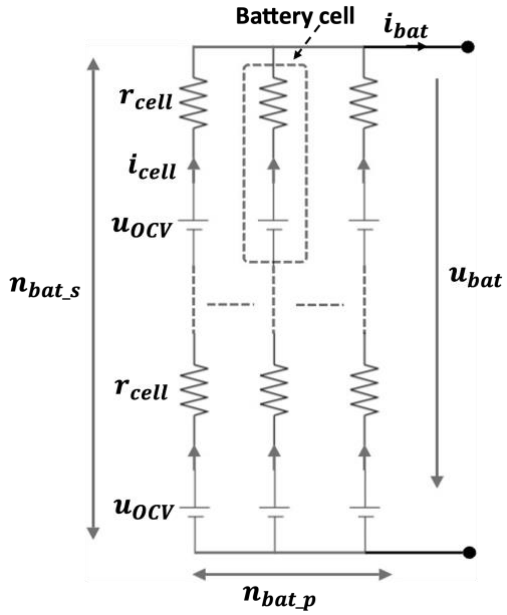


Figure 7.3: Battery pack equivalent circuit [62]

7.2 Generalised Port Crane H-ESS Sizing Framework

To find the optimal size of the battery and supercapacitor packs for the port crane, a generalised port crane H-ESS sizing framework is developed and is shown in Figure 7.4. The sizing framework inputs the crane's load speed profile into the port crane EMR model, which has an optimal EMS. The optimal EMS outputs the optimal battery and supercapacitor current profiles, which are taken as inputs into the PSO-based H-ESS sizing algorithm. The optimisation-based particle swarm algorithm (PSO) is used to determine the optimal battery and supercapacitor sizes. The port crane H-ESS sizing framework shown in Figure 7.4 produces an optimally sized battery/supercapacitor H-ESS for port cranes by using optimisation-based methods in both the framework's energy management and sizing layers. Furthermore, this framework is a generalised framework that can be applied to other types of cranes by using the particular crane load profile and parameters in the equations.

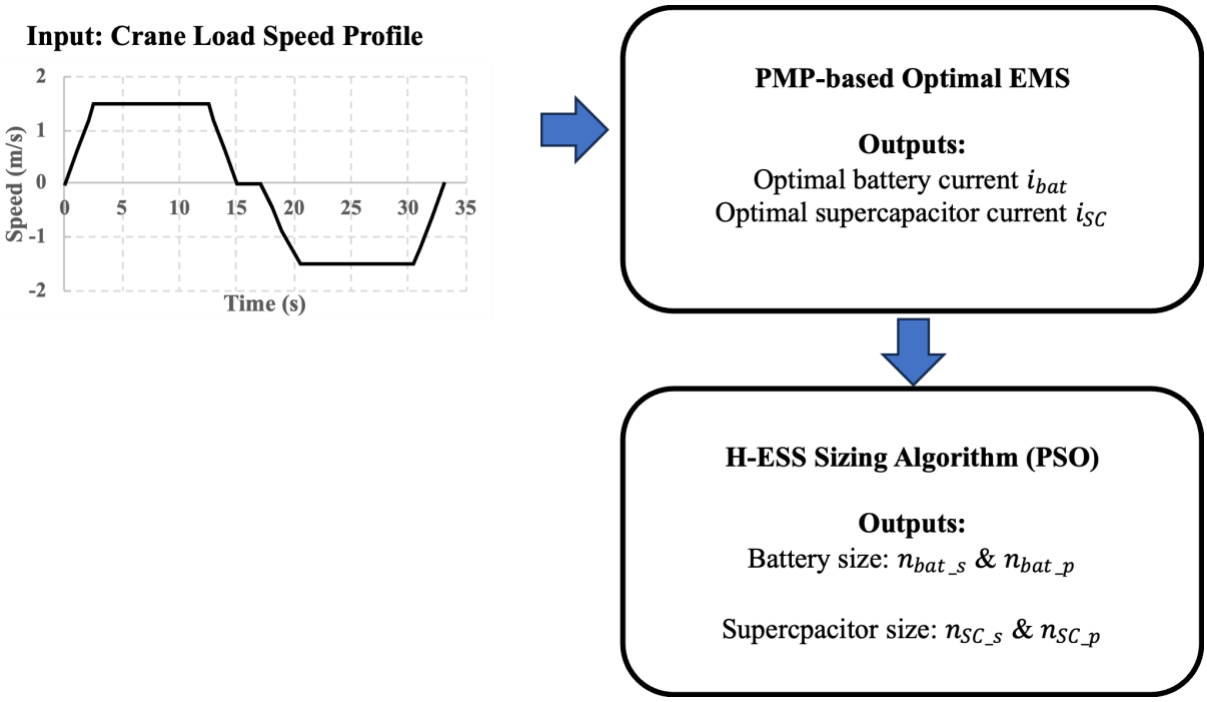


Figure 7.4: Generalised port crane H-ESS sizing framework

7.3 Generalised H-ESS Sizing Problem Formulation

The generalised sizing framework aims to find the optimal size of the battery and supercapacitor packs that simultaneously optimise energy consumption and HESS cost. Figure 7.2 shows that the battery size is determined by the parameters n_{bat_s} and n_{bat_p}. Similarly, Figure 7.3 shows that the size of the supercapacitor pack is determined by the parameters n_{SC_s} and n_{SC_p}. These four parameters are, therefore, the main focus of the optimal sizing H-ESS problem as they are the variables related to the port crane energy system performance and operation.

Figure 7.4 shows the main components required for implementing the generalised port crane H-ESS sizing framework. The input crane load speed profile is determined from the crane design. In chapter 6, the optimal battery and supercapacitor currents are determined using the PMP algorithm in equation (6.32). The work done in Chapter 6 completes the first objective of this chapter which is to optimize the crane's energy consumption. The results of the optimal currents from Chapter 6 are used as input into the H-ESS sizing algorithm in this chapter.

To complete the main components of the generalised port crane H-ESS sizing framework, this chapter develops the PSO-based H-ESS sizing algorithm. The PSO algorithm is used to solve the second objective in the generalised H-ESS sizing framework which is to minimise the cost of the H-ESS. In transportation systems, and particularly the port industry, minimising investment costs is crucial for reducing product prices and increasing profits. Therefore, the H-ESS cost should be kept as low as possible. The HESS cost which includes only the battery and supercapacitor costs, is calculated by equation (7.8), with the goal of minimising this economic function. Minimizing this cost function leads to finding the optimal values of the variables n_{bat_s} ,n_{bat_p}, n_{SC_s}, and n_{SC_p}, these four variables determine the optimal size of the battery and supercapacitor packs.

$$J_{cost} = Cost = C_{module} n_{sc_s} n_{sc_p} + C_{cell} n_{bat_s} n_{bat_p} \tag{7.8}$$

where C_{module} and C_{cell} are the supercapacitor module and battery cell price, respectively.

7.4 Constraints

The constraints define the boundaries of the energy storage system and the user demands, ensuring that the proposed configurations remain within acceptable limits. Primarily, the H-ESS design must meet the necessary power and energy demands of the powertrain system as follows:

$$\begin{cases} P_{\text{bat}} + P_{SC} = P_{HESS} \\ \dfrac{dE_{SC}}{dt} = -\eta^{-k_{SC}}(P_{HESS} - P_{bat}) \end{cases} \tag{7.9}$$

where η and E_{SC} are the efficiency and energy capacity of the supercapacitor pack, respectively. When the supercapacitor is discharging k_{SC} equals 1 and when it is charging it equals -1. P_{HESS} is determined in Chapter 6 based on the optimal battery and supercapacitor currents.

The battery and supercapacitor voltage limits are the second constraint as follows:

$$U_{x_min} \leq U_{x_nominal} \leq U_{x_max} \tag{7.10}$$

Where $U_{x_nominal}$ is the nominal value, U_{x_min} and U_{x_max} are the limits of the supercapacitor and battery voltages, respectively. As shown in Chapter 6, the battery controls the dc-bus voltage, therefore, the supercapacitor voltage is bound by the battery voltage limits.

In summary, the HESS optimal sizing problem is defined as follows:

Algorithm 7.1: H-ESS Optimal Sizing Problem Summary

Given optimal battery and supercapacitor currents i_{bat} and i_{SC}

min $f(\mathbf{z}) = J_{cost} = C_{module} n_{sc_s} n_{sc_p} + C_{cell} n_{bat_s} n_{bat_p}$

s.t.

$\mathbf{z} = (n_{bat_s}, n_{bat_p}, n_{SC_s}, n_{SC_p})$

$n_{bat_s}, n_{bat_p}, n_{SC_s}, n_{SC_p} \in \mathbb{N}^*$

Equality constraint (7.9)

Inequality constraint (7.10)

7.5 PSO H-ESS Sizing Algorithm

Given the optimal battery and supercapacitor currents as deduced in Chapter 6, the PSO algorithm is used to find the variables $n_{bat_s}, n_{bat_p}, n_{SC_s}$, and n_{SC_p} which determine the battery and supercapacitor sizes. The PSO algorithm is defined by its mathematical model, which includes the particle's current position and velocity vector, with the position determined by:

$$\overrightarrow{X_i^{t+1}} = \overrightarrow{X_i^t} + \overrightarrow{V_i^{t+1}} \tag{7.11}$$

The velocity of this particle's position is determined by:

$$\overrightarrow{V_i^{t+1}} = w\overrightarrow{V_i^t} + c_1 r_1 \left(\overrightarrow{P_i^t} - \overrightarrow{X_i^t}\right) + c_2 r_2 \left(\overrightarrow{G^t} - \overrightarrow{X_i^t}\right) \tag{7.12}$$

The following pseudocode outlines the PSO algorithm [51]:

Algorithm 7.2: Generalised PSO H-ESS Sizing Algorithm

Initialise the optimisation problem parameters

$fobj = objective\ function$ - *Equation* (7.8)

Initialise the PSO hyper-parameters (N, c1, c2, Wmin, Wmax, Vmax, and MaxIter)

Initialise the population of *N* particles

do

for each particle

calculate the fitness of the particle using objective function equation (7.8)

Update PBEST if required

Update GBEST if required

end for

Update the inertia weight

for each particle

Update the velocity (V)

Update the position (X)

end for

while the end condition is not satisfied

Return GBEST as the best estimation of the global optimum

7.6 Simulation Results

MATLAB simulations were conducted to determine the optimal port crane H-ESS size. The simulations followed the generalised port crane H-ESS sizing framework shown in Figure 7.4. The Panasonic battery cell NCR18650GA and the BCAP0350 E270 T11/13 supercapacitor module from [62] were selected for the H-ESS design, and their parameters are shown in Table 7.1. The cost of the selected battery and supercapacitor cells are in line with the latest levelized costs shown in [63].

Table 7.1: Supercapacitor module and battery cell parameters [62]

Parameter	Unit	Battery Cell	Supercapacitor Module
Maximum discharge current	A	10	170
Maximum charging current	A	3.45	170
Price	USD	2.7	30
Weight	g	48	60
Width	mm	18.5	33.3
Length	mm	18.5	33.3
Height	mm	65.3	61.5
Nominal voltage	V	3.6	2.7
Nominal capacity	Ah	3.3	–
Rated capacitance	F	–	350

First, the optimal crane energy consumption was determined, which led to the optimal battery and supercapacitor current requirements shown in Figure 7.5. The PMP-based EMS developed in Section 6.3 is used to deduce the optimal currents. The optimal current profiles are then used as inputs into the PSO H-ESS sizing algorithm to determine the battery and supercapacitor sizes.

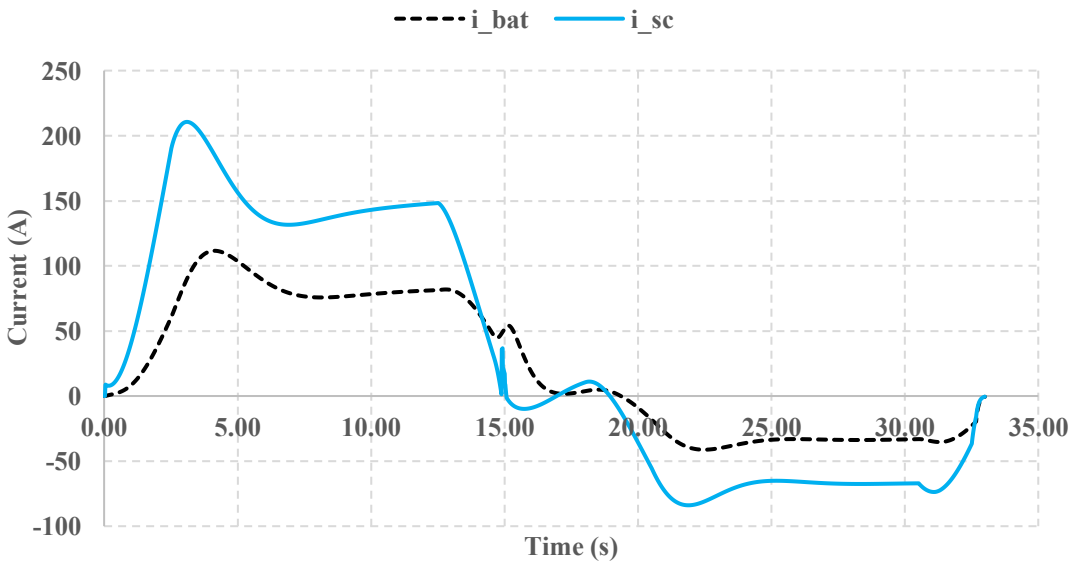


Figure 7.5: Optimal battery and supercapacitor currents

The second step was to determine the optimal port crane H-ESS size. Table 7.2 presents the simulated optimal battery and supercapacitor sizes and their associated H-ESS cost. Because the port crane is larger than 2 MW, the results indicate that very large battery and supercapacitor sizes can be used. Although the supercapacitor pack is smaller in size, it is more costly than the battery pack. The cost of H-ESS components corresponds to the optimized current profiles depicted in Figure 7.5 reflecting the characteristics of the energy storage devices. Specifically, the smaller supercapacitor predominantly manages energy during crane acceleration and deceleration phases, while the battery is responsible for energy supply and recovery during steady-state operation of the crane load profile. Figure 7.6 and Figure 7.7 shows that, as expected, as the battery and supercapacitor sizes increase, so does the cost of the H-ESS, highlighting the trade-offs involved in sizing decisions.

Table 7.2: Simulated battery and supercapacitor sizes

Battery		**Supercapacitor**		**Battery Cost (USD)**	**Supercapacitor Cost (USD)**	**Total H-ESS Cost (USD)**
Series modules (n_{bat_s})	Parallel branches (n_{bat_p})	Series modules (n_{SC_s})	Parallel branches (n_{SC_p})			
72	62	18	41	$12,032.08	$22,757.28	$34,789.36
22	50	18	37	$2,929.21	$20,064.93	$22,994.14
51	48	7	39	$6,548.96	$7,978.16	$14,527.12

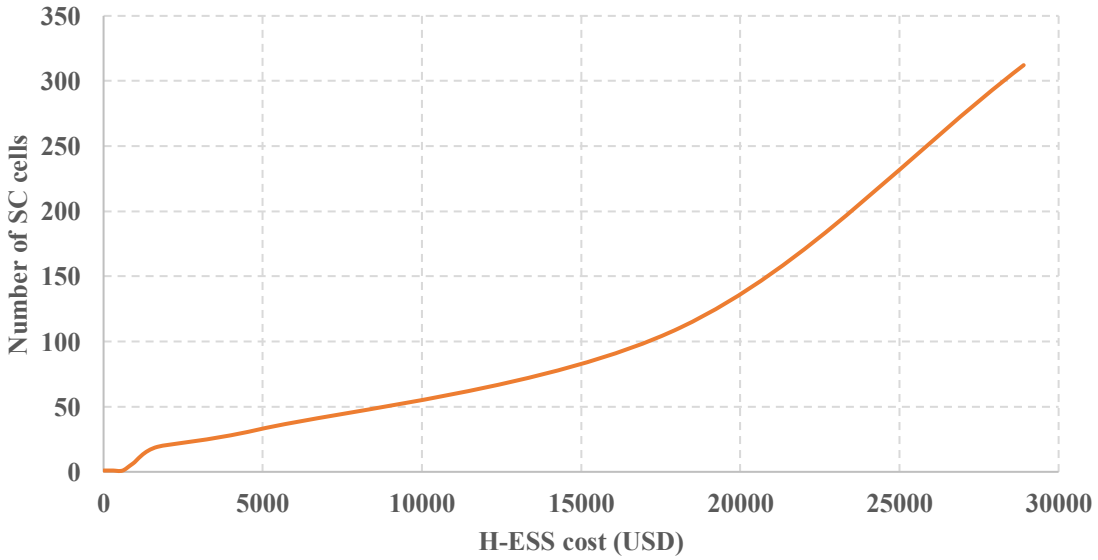


Figure 7.6: Supercapacitor size vs. H-ESS cost

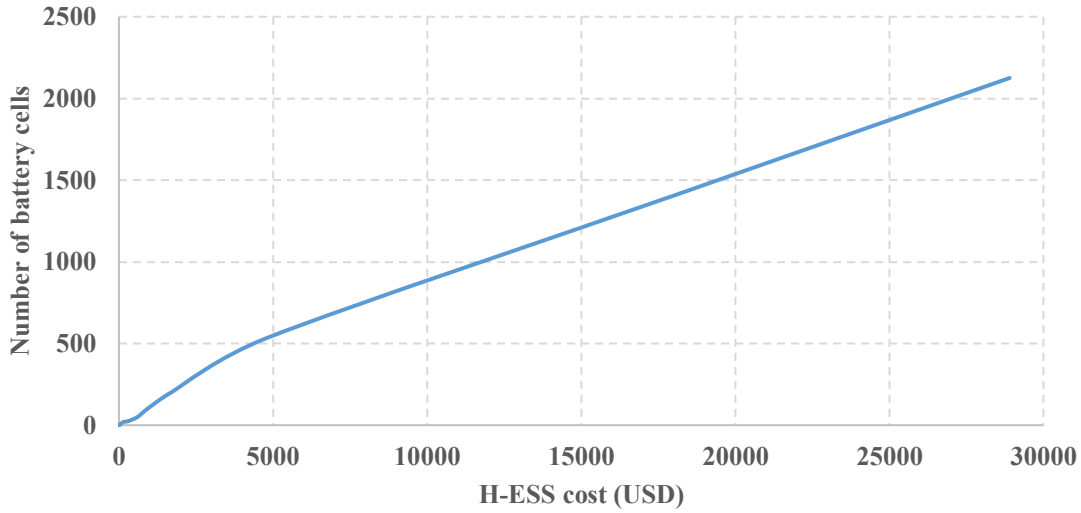


Figure 7.7: Battery size vs. H-ESS cost

Lastly, Figure 7.8 shows that the PSO H-ESS sizing algorithm convergences in a few iterations to find the H-ESS optimal cost. Therefore, the PSO H-ESS sizing algorithm is demonstrated to be computationally efficient and less complex, which is an advantageous feature given the variety of port cranes. The validity of the results in this chapter is supported by the fact that the optimal crane current profiles were generated using the crane model validated in Section 4.6. Additionally, the costs of H-ESS components are based on their levelized cost of energy values. Overall, this chapter has demonstrated the application of the generalised port crane H-ESS sizing framework.

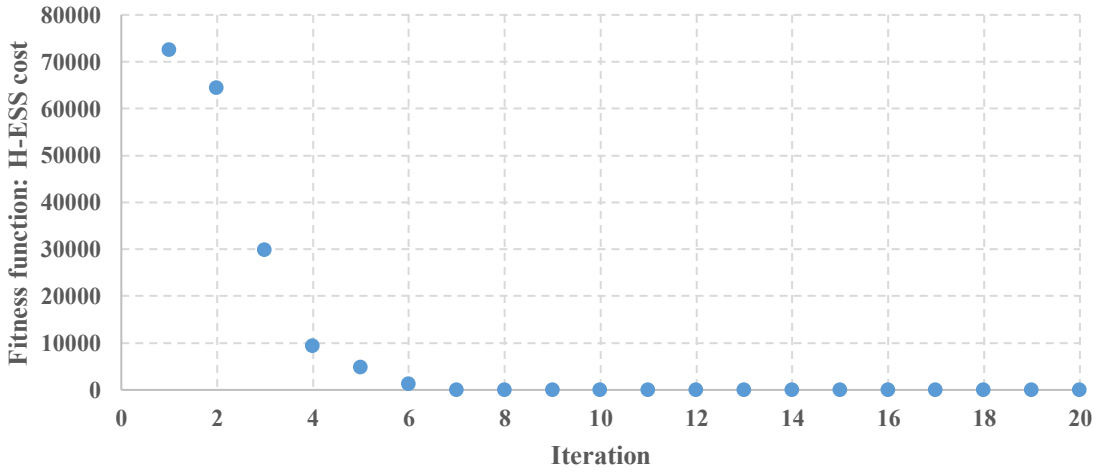


Figure 7.8: PSO H-ESS cost convergence plot

7.7 Chapter Summary

This chapter presents the optimal sizing methodology for port cranes' hybrid energy storage system (H-ESS), focusing on the battery and supercapacitor components. Using an optimisation-based approach, specifically a particle swarm optimisation (PSO) algorithm, the chapter determines the optimal sizes of these energy storage devices based on the crane's energy consumption profile and energy management strategy (EMS). The equivalent circuit models of both the battery and supercapacitor are described, followed by the implementation of a generalised sizing framework applicable to different crane types. Simulation results show that as battery and supercapacitor sizes increase, so does the overall H-ESS cost, highlighting the trade-offs involved in sizing decisions. Ultimately, the chapter demonstrates the effectiveness of the proposed generalised port crane H-ESS sizing framework in determining an optimised battery-supercapacitor combination.

8. Conclusions and Future Works

8.1 Conclusions

This study investigates the application of hybrid energy storage systems (H-ESS), particularly combinations of batteries and supercapacitors, and their potential for improving energy efficiency in port cranes. A key focus is the lack of detailed research on energy management for port cranes, especially using optimisation-based methods and optimal trajectories for energy and productivity improvements. The study adopts the EMR formalism for modelling the crane system, enabling the structured development of control systems and energy management strategies. The crane's EMR model was validated using real-world crane data and found to accurately reflect the crane's actual power consumption. The thesis combines an optimal load-handling trajectory with an optimisation-based EMS to manage energy usage effectively, validated through simulations in MATLAB/Simulink using real-world cranes.

First, the optimal load trajectory for port cranes was identified as a cycloidal path. The implementation of the optimal trajectory to the port crane produced the following results:

- The developed optimal crane load trajectory is 38.59% faster and more productive compared to the non-optimal trajectory.
- The optimal trajectory reduces the crane's peak power consumption by 36.38% relative to the non-optimal trajectory.
- The optimal trajectory reduces the crane's energy consumption by 26.67% compared to the non-optimal trajectory and by 10.81% compared to trajectories followed by experienced crane drivers.
- The sinusoidal speed reference curves derived from the cycloid trajectory can serve as a guide for automating port crane systems.
- The outcomes of this study provide guidelines for port crane designers, enabling the selection of cranes based on energy consumption requirements, maximum wind speed tolerance, crane lifting height, and the trolley distance between the ship and the shore.

Secondly, an energy management strategy for port cranes was developed. The objective of the EMS is to manage the energy distribution between the grid and an H-ESS which consists of both a battery and a supercapacitor. The sub-objective of the EMS is to extend battery life. The developed energy management strategy is a combination of filtering and Pontryagin Minimum Principle strategies. The results of applying the EMS and H-ESS to the port crane powertrain are as follows:

- The port crane's energy consumption from the utility grid decreased by 29%.
- The peak power consumption from the utility grid decreased by 29.6%.
- During the crane load handling cycle, the supercapacitor and the battery are discharged and recharged by 26% and 8%, respectively. The recharge is due to regenerative braking energy.
- Given that STS cranes are the largest port cranes with about 2 MW power demand and share a common drivetrain with many types of port and industry cranes, the EMS developed in this study is applicable to other types of cranes.

Overall, the proposed EMS model for this study has a simple analytical cost function, is computationally fast, and is easy to implement while producing optimal and effective results. Furthermore, the EMS enhances the performance of the H-ESS by boosting efficiency, improving reliability, and extending its lifespan, making H-ESS more dependable and cost-efficient. Lastly, the study developed a generalised port crane H-ESS sizing framework that uses the optimal EMS and the particle swarm optimisation (PSO) algorithm to determine the optimal sizes of the battery and supercapacitor packs in the H-ESS.

8.2 Recommendations for Future Works

This thesis focused on optimal trajectories and energy management strategies for port cranes. Future studies could extend this study by exploring the application of other energy storage technologies beyond the batteries and supercapacitors considered in this study. Additionally, future studies could further explore the optimal sizing of energy storage systems.

Bibliography

[1] M. Kotzampasakis, “Maritime emissions trading in the EU: Systematic literature review and policy assessment,” *Transp Policy (Oxf)*, vol. 165, pp. 28–41, May 2025, doi: 10.1016/J.TRANPOL.2025.02.014.

[2] R. Takalani and L. Masisi, “Development of an Optimal Port Crane Trajectory for Reduced Energy Consumption,” *Energies 2023, Vol. 16, Page 7172*, vol. 16, no. 20, p. 7172, Oct. 2023, doi: 10.3390/EN16207172.

[3] Ç. Iris and J. S. L. Lam, “A review of energy efficiency in ports: Operational strategies, technologies and energy management systems,” 2019. doi: 10.1016/j.rser.2019.04.069.

[4] G. Parise, C. Lien Su, K. Sayler, and P. Baratono, “An Electro-Energetic Guide for Planning & Operating of Port Systems,” *IEEE Trans Ind Appl*, 2024, doi: 10.1109/TIA.2024.3522215.

[5] F. M. Barbosa, A. Kullberg, and J. Löfberg, “Fast or Cheap: Time and Energy Optimal Control of Ship-to-Shore Cranes,” *IFAC-PapersOnLine*, vol. 56, no. 2, pp. 3126–3131, Jan. 2023, doi: 10.1016/J.IFACOL.2023.10.1445.

[6] Y. Liang, R. Li, T. Liu, C. Lin, T. Wang, and Y. He, “An enhanced coupling optimal trajectory planning for bridge cranes,” *Proc Inst Mech Eng C J Mech Eng Sci*, vol. 238, no. 6, pp. 2007–2017, Mar. 2024, doi: 10.1177/09544062231190797.

[7] M. Brenna *et al.*, “A Review on Energy Efficiency in Three Transportation Sectors: Railways, Electrical Vehicles and Marine,” *Energies 2020, Vol. 13, Page 2378*, vol. 13, no. 9, p. 2378, May 2020, doi: 10.3390/EN13092378.

[8] M. Waseem, G. S. Lakshmi, M. Ahmad, and M. Suhaib, “Energy storage technology and its impact in electric vehicle: Current progress and future outlook,” *Next Energy*, vol. 6, p. 100202, Jan. 2025, doi: 10.1016/J.NXENER.2024.100202.

[9] D. Zhang, W. Sun, Y. Zou, X. Zhang, and Y. Zhang, “An improved soft actor-critic-based energy management strategy of heavy-duty hybrid electric vehicles with dual-engine system,” *Energy*, vol. 308, p. 132938, Nov. 2024, doi: 10.1016/J.ENERGY.2024.132938.

[10] D. Vlahopoulos and A. S. Bouhouras, “Solution for RTG crane power supply with the use of a hybrid energy storage system based on literature review,” *Sustainable Energy Technologies and Assessments*, vol. 52, p. 102351, Aug. 2022, doi: 10.1016/J.SETA.2022.102351.

[11] A. Perrigot, M. Perier-Muzet, P. Ortega, F. Ferrucci, and D. Stitou, “Energetic macroscopic representation of a mechanical compression-assisted hybrid thermochemical cycle exploiting low grade heat for cold applications,” *Energy Convers Manag*, vol. 294, p. 117521, Oct. 2023, doi: 10.1016/J.ENCONMAN.2023.117521.

[12] B. H. Nguyen, R. German, J. P. F. Trovao, and A. Bouscayrol, “Real-time energy management of battery/supercapacitor electric vehicles based on an adaptation of pontryagin’s minimum principle,” *IEEE Trans Veh Technol*, vol. 68, no. 1, pp. 203–212, Jan. 2019, doi: 10.1109/TVT.2018.2881057.

[13] Z. Wu and X. Xia, “Optimal motion planning for overhead cranes,” *IET Control Theory and Applications*, vol. 8, no. 17, pp. 1833–1842, Nov. 2014, doi: 10.1049/iet-cta.2014.0069.

[14] N. Zhao, N. Schofield, and W. Niu, “Energy storage system for a port crane hybrid power-train,” *IEEE Transactions on Transportation Electrification*, vol. 2, no. 4, pp. 480–492, Dec. 2016, doi: 10.1109/TTE.2016.2562360.

[15] A. Bouscayrol, J. P. Hautier, and B. Lemaire-Semail, “Graphic Formalisms for the Control of Multi-Physical Energetic Systems: COG and EMR,” in *Systemic Design Methodologies for Electrical Energy Systems: Analysis, Synthesis and Management*, John Wiley and Sons, 2013, pp. 89–124. doi: 10.1002/9781118569863.ch3.

[16] B. Nguyen, “Energy management strategies of electric and hybrid vehicles supplied by hybrid energy storage systems,” Ph.D Thesis, Ph.D. Thesis, Faculté de Génie, Université de Sherbrooke, 2019.

[17] N. Zrnić, Z. Petković, and S. Bošnjak, “Automation of ship-to-shore container cranes: A review of state-of-the-art,” *FME Transactions*, vol. 33, no. 3, pp. 111–121, 2005.

[18] C. Chlomoudis and T. Styliadis, “Innovation and Patenting within Containerized Liner Shipping,” *Sustainability 2022, Vol. 14, Page 892*, vol. 14, no. 2, p. 892, Jan. 2022, doi: 10.3390/SU14020892.

[19] M. Kermani, E. Shirdare, G. Parise, M. Bongiorno, and L. Martirano, “A Comprehensive Technoeconomic Solution for Demand Control in Ports: Energy Storage Systems Integration,” *IEEE Trans Ind Appl*, vol. 58, no. 2, pp. 1592–1601, 2022, doi: 10.1109/TIA.2022.3145769.

[20] R. Takalani and L. Masisi, “Development of An Energy Management Strategy for Port Cranes,” in *IECON Proceedings (Industrial Electronics Conference)*, IEEE, 2021. doi: 10.1109/IECON48115.2021.9589271.

[21] F. R. Salmasi, “Control strategies for hybrid electric vehicles: Evolution, classification, comparison, and future trends,” *IEEE Trans Veh Technol*, vol. 56, no. 5 I, pp. 2393–2404, 2007, doi: 10.1109/TVT.2007.899933.

[22] Z. Song, H. Hofmann, J. Li, J. Hou, X. Han, and M. Ouyang, “Energy management strategies comparison for electric vehicles with hybrid energy storage system,” *Appl Energy*, vol. 134, pp. 321–331, 2014.

[23] M. Böck, A. Stöger, and A. Kugi, “Efficient Generation of Fast Trajectories for Gantry Cranes with Constraints,” in *IFAC-PapersOnLine*, Elsevier, Jul. 2017, pp. 1937–1943. doi: 10.1016/j.ifacol.2017.08.386.

[24] D. Rimpas *et al.*, “Energy management and storage systems on electric vehicles: A comprehensive review,” *Mater Today Proc*, vol. 61, pp. 813–819, Jan. 2022, doi: 10.1016/j.matpr.2021.08.352.

[25] P. J. Corral-Vega, P. García-Trivi, ~ No, and L. M. Fern Andez-Ramírez, “Design, modelling, control and techno-economic evaluation of a fuel cell/supercapacitors powered container crane,” 2019, doi: 10.1016/j.energy.2019.115863.

[26] B. H. Nguyễn, T. Vo-Duy, C. Henggeler Antunes, and J. P. F. Trovão, “Multi-objective benchmark for energy management of dual-source electric vehicles: An optimal control approach,” *Energy*, vol. 223, 2021, doi: 10.1016/j.energy.2021.119857.

[27] N. Zhao, “Modelling and design of electric machines and associated components for more electric vehicles,” Ph.D. Thesis, School of Graduate Studies, McMaster University, 2017.

[28] W. Zhou, C. J. Cleaver, C. F. Dunant, J. M. Allwood, and J. Lin, “Cost, range anxiety and future electricity supply: A review of how today’s technology trends may influence the future uptake of BEVs,” *Renewable and Sustainable Energy Reviews*, vol. 173, Mar. 2023, doi: 10.1016/j.rser.2022.113074.

[29] S. M. Kim and S. K. Sul, “Control of rubber tyred gantry crane with energy storage based on supercapacitor bank,” *IEEE Trans Power Electron*, vol. 21, no. 5, pp. 1420–1427, 2006, doi: 10.1109/TPEL.2006.880260.

[30] J. Yin, X. Peng, J. He, Q. Huo, and T. Wei, “Energy Management Method of a Hybrid Energy Storage System Combined With the Transportation-Electricity Coupling Characteristics of Ports,” *IEEE Transactions on Intelligent Transportation Systems*, 2023, doi: 10.1109/TITS.2023.3303497.

[31] M. Kermani, G. Parise, L. Martirano, L. Parise, and B. Chavdarian, “Utilization of Regenerative Energy by Ultracapacitor Sizing for Peak Shaving in STS Crane,” in

Proceedings - 2019 IEEE International Conference on Environment and Electrical Engineering and 2019 IEEE Industrial and Commercial Power Systems Europe, EEEIC/I and CPS Europe 2019, Institute of Electrical and Electronics Engineers Inc., Jun. 2019. doi: 10.1109/EEEIC.2019.8783770.

[32] G. Parise, A. Honorati, L. Parise, and L. Martirano, "Near zero energy load systems: The special case of port cranes," in *2015 IEEE/IAS 51st Industrial and Commercial Power Systems Technical Conference, I and CPS 2015*, 2015. doi: 10.1109/ICPS.2015.7266430.

[33] E. Vichos, N. Sifakis, and T. Tsoutsos, "Challenges of integrating hydrogen energy storage systems into nearly zero-energy ports," *Energy*, vol. 241, Feb. 2022, doi: 10.1016/j.energy.2021.122878.

[34] M. Kermani, G. Parise, L. Martirano, L. Parise, and B. Chavdarian, "Power balancing in STS group cranes with flywheel energy storage based on DSM strategy," *2018 IEEE 59th Annual International Scientific Conference on Power and Electrical Engineering of Riga Technical University, RTUCON 2018 - Proceedings*, 2018.

[35] X. Wang, J. Liu, X. Dong, H. Peng, and C. Li, "An energy-time optimal autonomous motion control framework for overhead cranes in the presence of obstacles," *https://doi.org/10.1177/0954406220954502*, vol. 235, no. 13, pp. 2373–2385, Sep. 2020, doi: 10.1177/0954406220954502.

[36] W. Zhang, H. Chen, H. Chen, and W. Liu, "A Time Optimal Trajectory Planning Method for Double-Pendulum Crane Systems with Obstacle Avoidance," *IEEE Access*, vol. 9, pp. 13022–13030, 2021, doi: 10.1109/ACCESS.2021.3050258.

[37] M. Masih-Tehrani, M. Ha'iri-Yazdi, V. Esfahanian, and A. Safae, "Optimum sizing and optimum energy management of a hybrid energy storage system for lithium battery life improvement," *J Power Sources*, vol. 244, pp. 2–10, 2013.

[38] B. H. Nguyen, T. Vo-Duy, M. C. Ta, and J. P. F. Trovao, “Optimal Energy Management of Hybrid Storage Systems Using an Alternative Approach of Pontryagin’s Minimum Principle,” *IEEE Transactions on Transportation Electrification*, 2021, doi: 10.1109/TTE.2021.3063072.

[39] X. Sun, J. Fu, H. Yang, M. Xie, and J. Liu, “An energy management strategy for plug-in hybrid electric vehicles based on deep learning and improved model predictive control,” *Energy*, vol. 269, Apr. 2023, doi: 10.1016/j.energy.2023.126772.

[40] Z. Yuan, L. Teng, S. Fengchun, and H. Peng, “Comparative Study of Dynamic Programming and Pontryagin’s Minimum Principle on Energy Management for a Parallel Hybrid Electric Vehicle,” *Energies 2013, Vol. 6, Pages 2305-2318*, vol. 6, no. 4, pp. 2305–2318, Apr. 2013, doi: 10.3390/EN6042305.

[41] O. Sundström and L. Guzzella, “A generic dynamic programming Matlab function,” *Proceedings of the IEEE International Conference on Control Applications*, pp. 1625–1630, 2009, doi: 10.1109/CCA.2009.5281131.

[42] A. Bouscayrol, B. Davat, B. De Fornel, … B. F.-T. E. physical, and undefined 2000, “Multi-converter multi-machine systems: application for electromechanical drives,” *epjap.org*, Accessed: Oct. 09, 2023. [Online]. Available: https://www.epjap.org/articles/epjap/abs/2000/05/ap9133/ap9133.html

[43] A. Castaings, W. Lhomme, R. Trigui, and A. Bouscayrol, “Comparison of energy management strategies of a battery/supercapacitors system for electric vehicle under real-time constraints,” *Appl Energy*, vol. 163, pp. 190–200, 2016, doi: 10.1016/j.apenergy.2015.11.020.

[44] B. H. Nguyên, J. P. Trovão, R. German, and A. Bouscayrol, “An Optimal Control-Based Strategy for Energy Management of Electric Vehicles Using Battery/Supercapacitor,” in *2017 IEEE Vehicle Power and Propulsion Conference, VPPC 2017 - Proceedings*, 2018, pp. 1–6. doi: 10.1109/VPPC.2017.8330985.

[45] W. Lhomme, A. Bouscayrol, S. A. Syed, S. Roy, F. Gailly, and O. Pape, “Energy Savings of a Hybrid Truck Using a Ravigneaux Gear Train,” *IEEE Trans Veh Technol*, vol. 66, no. 10, pp. 8682–8692, 2017, doi: 10.1109/TVT.2017.2710378.

[46] C. Boyer and U. Merzbach, *A history of mathematics*. 2011. Accessed: Sep. 06, 2023. [Online]. Available: https://books.google.com/books?hl=en&lr=&id=V6RUDwAAQBAJ&oi=fnd&pg=PR11&dq=xBoyer,+C.+B.+and+Merzbach,+U.+C.+A+History+of+Mathematics,+2nd+ed.+New+York:+Wiley,+1991.&ots=idcp5snRlX&sig=cAXKMpYKAn0d57EkVn6s5gM2CSQ

[47] V. Perlick, “The brachistochrone problem in a stationary space-time,” *J Math Phys*, vol. 32, no. 11, pp. 3148–3157, Nov. 1991, doi: 10.1063/1.529472.

[48] N. Sun, Y. Fang, Y. Zhang, and B. Ma, “A novel kinematic coupling-based trajectory planning method for overhead cranes,” *IEEE/ASME Transactions on Mechatronics*, vol. 17, no. 1, pp. 166–173, Feb. 2012, doi: 10.1109/TMECH.2010.2103085.

[49] N. Ashby, W. E. Brittin, W. F. Love, and W. Wyss, “Brachistochrone with Coulomb friction,” *Am J Phys*, vol. 43, no. 10, pp. 902–906, Oct. 1975, doi: 10.1119/1.9976.

[50] W. Pedrycz, A. Sillitti, and G. Succi, “Computational intelligence: An introduction,” *Studies in Computational Intelligence*, vol. 617, pp. 13–31, Jan. 2016, doi: 10.1007/978-3-319-25964-2_2.

[51] R. Poli, J. Kennedy, and T. Blackwell, “Particle swarm optimization: An overview,” *Swarm Intelligence*, vol. 1, no. 1, pp. 33–57, Aug. 2007, doi: 10.1007/s11721-007-0002-0.

[52] The World Bank, “TRANSPORT GLOBAL PRACTICE. The Container Port Performance Index 2021. A Comparable Assessment of Container Port Performance.,” 2021.

[53] H. Maghfiroh, O. Wahyunggoro, A. C.-P.-A. in Electrical, and undefined 2024, "Novel iterative Ragone plot-based optimization of low pass filter for hybrid power sources electric vehicles," *Elsevier*, Accessed: May 07, 2024. [Online]. Available: https://www.sciencedirect.com/science/article/pii/S277267112300284X

[54] A. Nguyen, J. Lauber, M. D.-E. C. and Management, and undefined 2014, "Optimal control based algorithms for energy management of automotive power systems with battery/supercapacitor storage devices," *ElsevierAT Nguyen, J Lauber, M DambrineEnergy Conversion and Management, 2014•Elsevier*, vol. 87, pp. 410–420, 2014, doi: 10.1016/j.enconman.2014.07.042ï.

[55] A. E. Bryson and Y.-C. Ho, "Applied Optimal Control," *Applied Optimal Control*, May 2018, doi: 10.1201/9781315137667/APPLIED-OPTIMAL-CONTROL-BRYSON.

[56] S. Günther, L. Weber, … A. B.-I., and undefined 2022, "Structured analysis and review of filter-based control strategies for hybrid energy storage systems," *ieeexplore.ieee.orgS Günther, L Weber, AL Bensmann, R Hanke-RauschenbachIEEE Access, 2022•ieeexplore.ieee.org*, Accessed: Sep. 01, 2024. [Online]. Available: https://ieeexplore.ieee.org/abstract/document/9968259/

[57] X. Gao, L. F.-I. Access, and undefined 2020, "SOC optimization based energy management strategy for hybrid energy storage system in vessel integrated power system," *ieeexplore.ieee.orgX Gao, L FuIEEE Access, 2020•ieeexplore.ieee.org*, Accessed: Sep. 01, 2024. [Online]. Available: https://ieeexplore.ieee.org/abstract/document/9039671/

[58] B. Taye, N. C.-P.-A. in E. Engineering, and undefined 2023, "Adaptive filter based method for hybrid energy storage system management in DC microgrid," *Elsevier*, Accessed: Aug. 31, 2024. [Online]. Available: https://www.sciencedirect.com/science/article/pii/S2772671123001547

[59] P. Thounthong and S. Raël, “The benefits of hybridization: An investigation of fuel cell/battery and fuel cell/supercapacitor hybrid sources for vehicle applications,” *IEEE Industrial Electronics Magazine*, vol. 3, no. 3, pp. 25–37, 2009, doi: 10.1109/MIE.2009.933885.

[60] A. Allègre, … A. B.-I. E. S. in, and undefined 2013, “Flexible real-time control of a hybrid energy storage system for electric vehicles,” *Wiley Online LibraryAL Allègre, A Bouscayrol, R TriguiIET Electrical Systems in Transportation, 2013•Wiley Online Library*, vol. 3, no. 3, pp. 79–85, 2012, doi: 10.1049/iet-est.2012.0051.

[61] A. Florescu, S. Bacha, I. Munteanu, … A. B.-J. of P., and undefined 2015, “Adaptive frequency-separation-based energy management system for electric vehicles,” *ElsevierA Florescu, S Bacha, I Munteanu, AI Bratcu, A RumeauJournal of Power Sources, 2015•Elsevier*, Accessed: May 07, 2024. [Online]. Available: https://www.sciencedirect.com/science/article/pii/S0378775315001330

[62] T. Nguyen-Minh, B. H. Nguyễn, T. Vo-Duy, M. C. Ta, J. P. F. Trovão, and C. H. Antunes, “A universal optimal sizing for hybrid energy storage system of electric vehicles,” *J Energy Storage*, vol. 92, p. 112128, Jul. 2024, doi: 10.1016/J.EST.2024.112128.

[63] N. G. Chatzigeorgiou, S. Theocharides, G. Makrides, and G. E. Georghiou, “A review on battery energy storage systems: Applications, developments, and research trends of hybrid installations in the end-user sector,” *J Energy Storage*, vol. 86, May 2024, doi: 10.1016/j.est.2024.111192.